Journal of Sound and Vibration 366 (2016) 149–172

Contents lists available at ScienceDirect

Journal of Sound and Vibration

journal homepage: www.elsevier.com/locate/jsvi

Reconstructing blockages in a symmetric duct *via* quasi-isospectral horn operators

Antonio Bilotta [a], Antonino Morassi [b,1], Emilio Turco [c,*]

[a] Università della Calabria, Dipartimento di Ingegneria Informatica, Modellistica, Elettronica e Sistemistica - DIMES, Via P. Bucci, 87036 Rende, CS, Italy
[b] Università degli Studi di Udine, Dipartimento Politecnico di Ingegneria e Architettura, via Cotonificio 114, 33100 Udine, UD, Italy
[c] Università degli Studi di Sassari, Dipartimento di Architettura, Design e Urbanistica, Asilo Sella, via Garibaldi 35, 07041 Alghero, SS, Italy

ARTICLE INFO

Article history:
Received 1 May 2015
Received in revised form
12 December 2015
Accepted 18 December 2015
Handling Editor: R.E. Musafir
Available online 4 January 2016

Keywords:
Horn equation
Blockage identification
Inverse problems in acoustics
Numerical modelling
Reconstruction
Quasi-isospectral Sturm-Liouville operators

ABSTRACT

This paper proposes a new method for the reconstruction of the blockage area function in a symmetric duct by resonant frequencies under a given set of end conditions, *i.e.*, open–open or closed–closed ends. The analysis is based on the explicit determination of quasi-isospectral ducts, that is duct profiles which have the same spectrum as a given duct with the exception of a single eigenfrequency which is free to move in a prescribed interval. The analytical reconstruction was numerically implemented and tested for the detection of blockages. Numerical results show that the accuracy of identification increases with the number of eigenfrequencies used and that the reconstruction is rather stable with respect to the shape, the size and the position of the blockages.

1. Introduction

The identification of the cross-sectional area variation induced by the occurrence of blockages in a duct or in a pipe by using non-intrusive acoustic measurements is an important issue in several contexts. Applications range from detection of blockages in sodium cooled fast reactors [1] to diagnostic analysis of piped fluid systems. Other research works concern the use of classical acoustic methods based on impedance testing for the identification of cross-sectional area changes in vocal tracts or ear canals [2,3], although more efficient approaches have been recently developed for the analysis of these inherently dissipative systems, see, for example, [4,5]. Among advanced applications in the field, the research developed by Campbell and co-workers on the use of Acoustic Pulse Reflectometry for determining the internal dimensions of musical wind instruments [6] and for leak detection in tubular objects [7] should be also mentioned.

A commonly accepted approximation to the wave equation that governs the low-frequency sound propagation in a duct is Webster's horn equation [8]. The model considers the duct to be a slender hard-walled tube, lossless, and to have a rate of change of cross sectional area with the distance x along the tract that is sufficiently small, so that the sound pressure can be approximated by means of a longitudinal sound wave along the x-direction. For a sound pressure $p(x,t)$ varying harmonically in time with radian frequency ω, *i.e.*, $p(x,t)=u(x)e^{i\omega t}$, where i is the imaginary unit, the spatial propagation of the

* Corresponding author.
E-mail addresses: antonio.bilotta@unical.it (A. Bilotta), antonino.morassi@uniud.it (A. Morassi), emilio.turco@uniss.it (E. Turco).
[1] Tel.: +39 0432 558739; fax: +39 0432 558700.

http://dx.doi.org/10.1016/j.jsv.2015.12.038
0022-460X/

longitudinal acoustic wave of small amplitude $u(x)$ is governed by the Webster horn operator

$$(A(x)u'(x))' + \lambda A(x)u(x) = 0, \quad \text{in } (0,L), \quad \lambda = \frac{\omega^2}{c_s^2}, \tag{1.1}$$

where $A = A(x)$ is the cross-sectional area, L is the duct length, c_s is the velocity of sound, and the primes denote x-differentiation. We refer to [9] for a rigorous derivation of Webster's horn equation based on the method of slow variation and ideas of matched asymptotic expansions. The boundary value problem is completed by assigning the conditions at the ends of the duct, namely the classical limit conditions $u' = 0$ for a closed end and $u = 0$ for an open end; see [9] for a rigorous asymptotic derivation of the boundary conditions and for a deep analysis of the boundary layer at the ends of slowly varying ducts. Under given (classical) end conditions at $x = 0$ and $x = L$, there exists a denumerable family of eigenvalues $\{\lambda_m\}_{m=1}^{\infty}$ (and eigenfrequencies, or resonant frequencies, ω_m) of Eq. (1.1), which form the *spectrum* of the duct. The corresponding non-trivial solutions u_m to Eq. (1.1) are the normal modes of vibration, or eigenfunctions, of the duct.

An important question is whether the shape $A(x)$ of a blockage perturbed duct can be determined from its resonant frequencies.

From the mathematical point of view, it has been shown that knowledge of two complete spectra, having specific asymptotic forms and satisfying specific interlacing conditions, correspondent to two different end conditions of the duct (*i.e.*, closed–closed and closed–open ends) uniquely determines the cross-sectional area $A(x)$, up to a multiplicative factor, see [10–12]. Knowledge or measurement of the doubly infinite set of eigenvalues is not realistic, since it is only for low frequencies that Webster's horn equation properly models the sound propagation in a duct. Therefore, in practical applications, the attention must be necessarily restricted to a set of lowest-order eigenvalues.

Reconstruction of the cross-sectional area from a finite number of (lower) eigenfrequency data has been carried out in the literature using perturbation analysis. On assuming that the unknown cross-sectional area $A(x)$ is a smooth perturbation of the uniform closed–open duct A_0 and that the logarithm of the normalized area function variation $\ln(A(x)/A_0)$ is band limited in frequency preserving only $2N$ cosine Fourier components, *e.g.*, $\ln(A(x)/A_0) = \sum_{j=1}^{2N} a_j \cos\frac{2jx}{L}$, Mermelstein [3] proved that the first-order change of the mth eigenfrequency of the closed–open duct and the change of the mth eigenfrequency of the closed–closed duct determines uniquely the $(2m-1)$th and the $2m$th Fourier coefficient of $\ln(A(x)/A_0)$, respectively.

The perturbation approach proposed by Mermelstein was extended by Wu and Fricke [13] to the detection of blockages in ducts by eigenfrequency measurements on closed–open and closed–closed end conditions. The identification procedure by Wu and Fricke was still based on the assumption that the blockages are a perturbation of the original duct, but, different from previous studies, the identification concerned with less regular cross-sectional coefficients, since the duct profile was assumed to be a piecewise-constant function. In spite of this weak regularity, the agreement between calculated and actual blockage area was good when half-wavelength of the eigenfrequency measured is greater than the length of the blockage.

The above reconstruction methods require the knowledge of a set of eigenvalues coming from spectra corresponding to two different end conditions. The requirement to modify a boundary condition (from closed–open to closed–closed, for example) in order to obtain information on a second spectrum, could be deemed and could represent a limit for the concrete application of the identification method. De Salis and Oldham [14] noticed that the completion of the finite Fourier expansion of $\ln(A(x)/A_0)$ is possible by using measurements under a single set of boundary conditions. They observed that eigenfrequencies for the closed–closed duct coincide with the antiresonant frequencies of the driven frequency response function measured at the open end of the closed–open duct. Estimate of antiresonant frequencies requires specific experimental and signal-processing strategies in order to locate the frequency with accuracy. In a subsequent paper, De Salis and Oldham [15] proposed high noise immunity maximum length sequence techniques to estimate accurately the locations of the antiresonant frequencies in the measured frequency response, and applied their method to identify blockages in a duct.

All the available results on the determination of the duct cross-sectional area from eigenfrequency measurements are founded on the assumption that the unknown cross-sectional area is a small perturbation of the intact (or initial) duct. However, the smallness of the perturbation is never stated in a quantitative way, *i.e.*, in terms of a suitable norm of the cross-sectional area change function, and this makes it difficult to determine the error in the reconstruction of the unknown coefficient. Based on the results by Wu and Fricke [13], for example, the perturbation analysis seems to be valid for blockage with change of area less than 50 percent of the intact area and blockage length less than $\frac{L}{4}$. In addition, since the reconstruction based on finite spectral data is not unique, it is not clear how large is the set of cross-sectional area coefficients $A(x)$ which share exactly all the first N eigenfrequencies coming from both the spectra under different end conditions. The above questions have motivated our research, and this paper is a contribution to this inverse problem in acoustics.

In this research we consider the problem of determining the geometry of a duct with blockages from a single spectrum. In the first part of the paper we show how to explicitly construct the cross-sectional area such that the duct has exactly the prescribed (measured) values of the first N eigenfrequencies belonging to a single spectrum obtained under either open–open or closed–closed end conditions. The analysis is developed for a symmetric duct, *e.g.*, a duct with cross-sectional area $A(x) \in C^2([0,L])$ such that $A(x) = A(L-x)$. In this case, the knowledge of a single full spectrum determines uniquely the shape profile, up to a multiplicative constant [16]. Our method is based on the determination of the so-called quasi-isospectral horn operators which have exactly the same spectrum as a given horn, with the exception of a single eigenfrequency which is free to move in a prescribed interval. The coefficient $A(x)$ and the normal modes can be constructed explicitly by means of

closed-form expressions. The second part of the paper is devoted to the numerical implementation of the analytical procedure. The effectiveness of the reconstruction is assessed with respect to the number and the set of eigenfrequencies used, the blockage profile, and the presence of errors on the data. The results of the numerical simulations are encouraging and the method turns out to be sufficiently stable to errors on the measured data.

The plan of the paper is as follows. In Section 2 we present the theory. The numerical algorithm and the results of simulations are presented and discussed in Section 3 and in Section 4, respectively.

2. Theory

2.1. Main idea of the reconstruction procedure

The propagation of the longitudinal acoustic wave of small amplitude $u = u(x)$ and frequency ω in a thin horn of length L, under open–open end conditions, is governed by the normalized Webster horn equation

$$(\widehat{A}(x)u'(x))' + \lambda \widehat{A}(x)u(x) = 0, \quad x \in (0,1), \tag{2.1}$$

$$u(0) = 0 = u(1), \tag{2.2}$$

where $\lambda = \frac{\omega^2 L^2}{c_s^2}$, c_s is the sound velocity and $\widehat{A}(x)$ is the cross-sectional area at section of normalized abscissa x.

We shall assume throughout that $\widehat{A}(x)$ is a strictly positive, twice continuously differentiable function of x in $[0,1]$ and $\widehat{A}(x)$ is an even function of x with respect to $x = \frac{1}{2}$. We denote by $\{\lambda_m\}_{m=1}^{\infty}$ the infinite sequence of eigenvalues of Eq. (2.1), with $0 < \lambda_1 < \lambda_2 < \cdots$, $\lim_{m\to\infty} \lambda_m = \infty$.

The key point of our method is the explicit construction of a new (regular and even) horn profile $A = A(x)$ having the same eigenvalues as the given horn $\widehat{A}(x)$ under Dirichlet end conditions, with the exception of the nth eigenvalue, where n is a given integer, $n \geq 1$. We call these new horn operators $\frac{1}{A(x)}\frac{\mathrm{d}}{\mathrm{d}x}\left(A(x)\frac{\mathrm{d}}{\mathrm{d}x}\right)$, *quasi-isospectral* horn operators. Once we have a recipe for the construction of a quasi-isospectral horn operator, by keeping fixed all the eigenvalues λ_m with $m \neq n$ and moving the nth eigenvalue λ_n to the desired value, say $\tilde{\lambda}_n$, and using repeatedly the procedure, after N steps we will produce a horn with the first N given (*e.g.*, measured) eigenvalues $\{\tilde{\lambda}_m\}_{m=1}^{N}$.

We will see that the above reconstruction procedure needs the specification of an initial horn, whose eigenvalues must be close enough (in a way that can be rigorously specified) to those of the initial horn.

2.2. Quasi-isospectral horn operators under Dirichlet end conditions

The explicit determination of quasi-isospectral horn operators has been presented in [17] under open–closed end conditions, *e.g.*, $u(0) = 0 = u'(1)$. The analysis developed in [17] can be adapted to determine quasi-isospectral horn operators for open–open end conditions (corresponding to Dirichlet–Dirichlet end conditions in the case of longitudinally vibrating rods, see Section 9, point 1, of [17]). Referring to the above-mentioned paper for the details, we describe in the sequel the main results, which will be useful in the analysis.

Let us denote by

$$\widehat{A}(x) = \widehat{a}^2(x), \quad y(x) = \widehat{a}(x)u(x), \tag{2.3}$$

where $\widehat{a} = \widehat{a}(x)$ can be chosen of one-sign in $[0,1]$, say positive. Then, the eigenvalue problem ((Eqs. (2.1) and 2.2)) can be transformed to the Sturm–Liouville canonical form

$$y''(x) + \lambda y(x) = \widehat{q}(x)y(x), \quad x \in (0,1), \tag{2.4}$$

$$y(0) = 0 = y(1), \tag{2.5}$$

where the potential

$$\widehat{q}(x) = \frac{\widehat{a}''(x)}{\widehat{a}(x)}, \tag{2.6}$$

is a continuous function in $[0,1]$. Let us denote by $\{z_m\}_{m=1}^{\infty}$ the eigenfunctions of (Eqs. (2.4) and 2.5), normalized so that

$$z_m'(0) = 1, \quad m = 1, 2, \cdots. \tag{2.7}$$

Let n, $n \geq 1$, be a given integer and let $t \in \mathbb{R}$ be such that

$$\lambda_{n-1}(\widehat{q}) < \lambda_n(\widehat{q}) + t < \lambda_{n+1}(\widehat{q}), \tag{2.8}$$

with $\lambda_0(\widehat{q}) = 0$. Denote by $y_1 = y_1(x, \widehat{q}, \lambda_n + t)$, $y_2 = y_2(x, \widehat{q}, \lambda_n + t)$ the solutions to the initial value problems

$$y_1'' + (\lambda_n + t)y_1 = \widehat{q}y_1, \quad x \in (0,1), \tag{2.9}$$

$$y_1(0) = 1, \tag{2.10}$$

$$y_1'(0) = 0, \tag{2.11}$$

and

$$y_2'' + (\lambda_n + t) y_2 = \widehat{q} y_2, \quad x \in (0,1), \tag{2.12}$$

$$y_2(0) = 0, \tag{2.13}$$

$$y_2'(0) = 1. \tag{2.14}$$

Moreover, we introduce the function

$$w_{n,t}(x, \widehat{q}, \lambda_n + t) = y_1(x, \widehat{q}, \lambda_n + t) + \frac{y_1(1, \lambda_n) - y_1(1, \lambda_n + t)}{y_2(1, \lambda_n + t)} y_2(x, \widehat{q}, \lambda_n + t), \tag{2.15}$$

solution to

$$w_{n,t}'' + (\lambda_n + t) w_{n,t} = \widehat{q} w_{n,t}, \quad x \in (0,1), \tag{2.16}$$

$$w_{n,t}(0) = 1, \tag{2.17}$$

$$w_{n,t}(1) = y_1(1, \widehat{q}, \lambda_n), \tag{2.18}$$

for $t \neq 0$. Note that the function $w_{n,t}$ is well-defined for all $t \neq 0$ and has a removable singularity at $t=0$. Finally, let

$$\omega_{n,t}(x, \widehat{q}, \lambda_n + t) = [w_{n,t}, z_n], \tag{2.19}$$

where $[f,g] = fg' - f'g$, for every regular functions f and g. The function $\omega_{n,t}$ is a continuous and strictly positive function in $[0,1]$ for every $\widehat{q} \in C([0,1])$ and for every t satisfying Eq. (2.8), $n \geq 1$. Moreover, $\omega_{n,t}$ is a C^2-function of the variable x in $[0,1]$, see [18, p. 109].

Under the above notation, and by adapting the arguments shown in [17], it can be shown that for a given $n \geq 1$ the open–open horn with profile

$$A(x) = a^2(x), \tag{2.20}$$

where

$$a = \widehat{a} - t \frac{w_{n,t}}{\lambda_n \omega_{n,t}} [z_n, \widehat{a}], \quad \lambda_{n-1} < \lambda_n + t < \lambda_{n+1}, \tag{2.21}$$

has exactly the same eigenvalues $\{\lambda_m\}$ of the open–open horn $\widehat{A}(x) = \widehat{a}^2(x)$, with the exception of the nth, which is fixed to the value $\lambda_n + t$, *e.g.*, $\lambda_m(\widehat{A}) = \lambda_m(A)$ for every $m \geq 1$ with $m \neq n$, and $\lambda_n(A) = \lambda_n(\widehat{A}) + t$. The open–open horn $A = A(x)$ is the wished horn quasi-isospectral to the initial horn $\widehat{A} = \widehat{A}(x)$.

For the sake of completeness, we sketch the main steps of the construction of the profiles a's shown in Eq. (2.21). In a first step, the analysis is based on a double application of a Darboux lemma [19] to obtain potentials $q(x)$ quasi-isospectral to the initial potential $\widehat{q}(x)$ in the eigenvalue problem ((Eqs. (2.3) and 2.4)), see also [18]. Denote by L_r the standard Sturm–Liouville operator with potential $r \in C([0,1])$, *i.e.*, $L_r y = -y'' + ry$. Let μ and λ be two real numbers. In his simpler form, the Darboux lemma enables us to find a non-trivial solution z of a new equation $L_p z = \lambda z$ if we know a non-trivial solution g, f of the equation $L_r g = \mu g$, $L_r f = \lambda f$, respectively, corresponding to two different values λ, μ of the parameter and to the potential r. In particular, it turns out that $z = \frac{1}{g}[g,f]$ and $p = r - 2(\ln(g))''$. It should be noted that if g vanishes in $[0,1]$, then the expression of the potential p is understood to hold between the roots of g. These singular situations disappear by applying the Darboux lemma twice. Finally, in the second step, the double Darboux lemma is applied once more again to determine the expression (Eq. (2.21)) of a solution to $q = \frac{a''}{a}$, that is, to reconstruct the quasi-isospectral horn operator with profile $A(x) = a^2(x)$.

It should be noticed that the function $a = a(x)$ in Eq. (2.21) corresponds to a "physical" horn, since it can be proved that the function a is C^2-regular and strictly positive in $[0,1]$ for every value of t satisfying the two inequalities in Eq. (2.21). Moreover, if the initial horn profile $\widehat{A}(x)$ is an even function with respect to $x = \frac{1}{2}$, then, by merging the results in [17,18] (adapted for Dirichlet end conditions) it is possible to prove that also the corresponding quasi-isospectral horn profile $A(x)$ given by Eq. (2.20) is an even function with respect to $x = \frac{1}{2}$.

2.3. The reconstruction procedure

In this section we shall use previous results to show how to construct a horn which has prescribed values of the first N natural frequencies. We shall see that the reconstruction procedure needs the specification of a suitable *initial horn* and, therefore, the reconstruction procedure works if the horn to be determined is not very far (in a way that will be clarified in the sequel) from the initial horn.

Consider an open–open horn with given cross sectional profile $A_0(x) = a_0^2(x)$ and eigenvalues $\{\lambda_m(a_0)\}_{m=1}^{\infty}$, $0 < \lambda_1(a_0) < \lambda_2(a_0) < \cdots$. We now ask whether it is possible to construct from this horn a new horn having prescribed values

of the first N eigenvalues $\{\tilde{\lambda}_m\}_{m=1}^{N}$ under the same set of end conditions, with

$$0<\tilde{\lambda}_1<\tilde{\lambda}_2<\cdots<\tilde{\lambda}_N. \tag{2.22}$$

By the analysis of Section 2.2 we know how to construct from the horn $A_0(x)$ a new horn, say $A_1(x)=a_1^2(x)$, so that the Dirichlet eigenvalues $\{\lambda_m(a_0)\}$, $m\geq 2$, are kept fixed while $\lambda_1(a_1)$ is moving to the desired value $\tilde{\lambda}_1$. More precisely, by Eq. (2.21), the function $a_1=a_1(x)$ given by

$$a_1=a_0-t\frac{w_{1,t}}{\lambda_1(a_0)\omega_{1,t}}[z_1(a_0),a_0], \tag{2.23}$$

corresponds to a one-parameter family of horns such that

$$\lambda_m(a_1)=\lambda_m(a_0)+\delta_{m1}t, \tag{2.24}$$

$m\geq 1$, for t such that

$$0<\lambda_1(a_0)+t<\lambda_2(a_0). \tag{2.25}$$

If

$$\tilde{\lambda}_1<\lambda_2(a_0), \tag{2.26}$$

then we can determine the parameter t, say $t=t_1$, such that $\lambda_1(a_1)=\tilde{\lambda}_1$, *i.e.*,

$$t_1=\tilde{\lambda}_1-\lambda_1(a_0). \tag{2.27}$$

The horn $A_1=a_1^2$ has eigenvalues $\{\tilde{\lambda}_1,\lambda_2(a_0),\lambda_3(a_0),\ldots\}$, with $0<\tilde{\lambda}_1<\lambda_2(a_0)<\lambda_3(a_0)<\cdots$, and can be used as starting point for the next step of the procedure.

By repeating the same arguments, it is possible to modify a_1 so as to keep $\lambda_m(a_1)$ fixed for $m\neq 2$ and to move $\lambda_2(a_0)$ to the desired value $\tilde{\lambda}_2$, *i.e.*,

$$a_2=a_1-t_2\frac{w_{2,t_2}}{\lambda_2(a_0)\omega_{2,t_2}}[z_2(a_1),a_1], \tag{2.28}$$

where

$$t_2=\tilde{\lambda}_2-\lambda_2(a_0). \tag{2.29}$$

The eigenvalues of the new horn $a_2(x)$ are $\{\tilde{\lambda}_1,\tilde{\lambda}_2,\lambda_3(a_0),\lambda_4(a_0),\ldots\}$. Using repeatedly this procedure, after N steps we produce a horn, with cross-sectional profile area $A_N(x)=a_N^2(x)$, such that

$$\lambda_m(a_N)=\tilde{\lambda}_m,\quad \text{for } 1\leq m\leq N, \tag{2.30}$$

and the construction is finished. We note that the choice of the initial horn $a_0(x)$ is restricted by the conditions

$$\tilde{\lambda}_1<\lambda_2(a_0),\tilde{\lambda}_2<\lambda_3(a_0),\ldots,\tilde{\lambda}_{N-1}<\lambda_N(a_0),\tilde{\lambda}_N<\lambda_{N+1}(a_0), \tag{2.31}$$

which allow us to determine the numbers $t_1,t_2,\cdots,t_N$ by the expressions analogous to Eq. (2.27).

The above construction, which is based on a finite number of eigenfrequencies, is obviously not unique, since the flow from the initial horn a_0 to a horn with prescribed first N Dirichlet eigenvalues depends on the particular order chosen to move every individual eigenvalue to the target value. Similarly, the compatibility conditions on the initial horn a_0 may change depending on the sequence of eigenvalue shifts. For example, if we decide to move the N initial eigenvalues $\{\lambda_m(a_0)\}_{m=1}^{N}$ into the decided positions $\{\tilde{\lambda}_m\}_{m=1}^{N}$ beginning with $\lambda_N(a_0)$ and proceeding in descending order, the conditions (Eq. (2.31)) become

$$\lambda_{N-1}(a_0)<\tilde{\lambda}_N<\lambda_{N+1}(a_0),\lambda_{N-2}(a_0)<\tilde{\lambda}_{N-1},\ldots,\lambda_2(a_0)<\tilde{\lambda}_3,\lambda_1(a_0)<\tilde{\lambda}_2. \tag{2.32}$$

Concerning the uniqueness of the reconstruction when a full Dirichlet spectrum is specified, we recall that the complete set of eigenvalues $\{\lambda_m\}_{m=1}^{\infty}$ determines uniquely the potential $q(x)$, see [16]. Note that for a given $A(x)$ or $a(x)$, there is a unique $q(x)$, but for a given $q(x)$ there are many $a(x)$. In particular, if $a(x)$ is one $a(x)$ corresponding to a given $q(x)$, then all the coefficients $a^*(x)$ satisfying $q(x)=\frac{a^*(x)''}{a^*(x)}$ are given by

$$a^*(x)=a(x)\left(c_1+c_2\int_0^x\frac{\mathrm{d}s}{a^2(s)}\right), \tag{2.33}$$

where c_1 and c_2 are constants to be chosen so that $a^*(x)$ is one-sign (say, positive) in $[0,1]$. In our reconstruction method, the coefficient $a(x)$ is an even function with respect to $x=\frac{1}{2}$ and, therefore, $a^*(x)$ is an even function if and only if $c_2=0$. This implies that the knowledge of the full spectrum $\{\lambda_m\}_{m=1}^{\infty}$ determines uniquely $A(x)$, up to a multiplicative constant. In fact, as remarked in [13], a multiplicative constant on $A(x)$ has no effect on the eigenvalues. Therefore, in order to have uniqueness of the reconstruction as $N\to\infty$, we need to specify an additional information on $A(x)$, such as the average of $A(x)$ or, equivalently, the average of $A^{-1}(x)$.

2.4. An extension to closed–closed end conditions

In this section we consider the problem of constructing quasi-isospectral horn operators of the form Eq. (1.1) under closed–closed (or Neumann) end conditions. We recall the following simple, but useful, result.

Proposition 2.1. *Let $b \in C^2([0,1])$ a real-valued, strictly positive function in $[0,1]$. Let (λ, v) be an eigenpair of the Neumann problem*

$$(b^2 v')' + \lambda b^2 v = 0, \quad x \in (0,1), \tag{2.34}$$

$$v'(0) = 0 = v'(1). \tag{2.35}$$

(i) *If $\lambda \neq 0$, then λ, $\lambda > 0$, is an eigenvalue of the Dirichlet problem*

$$(a^2 u')' + \lambda a^2 u = 0, \quad x \in (0,1), \tag{2.36}$$

$$u(0) = 0 = u(1), \tag{2.37}$$

with

$$u = b^2 v', \quad a = b^{-1}, \quad x \in [0,1]. \tag{2.38}$$

(ii) *If (λ, u) is an eigenpair of the Dirichlet problem (Eq. (2.36)) for a real-valued, strictly positive function $a \in C^2([0,1])$, then λ, $\lambda > 0$, is an eigenvalue of the Neumann problem* (Eqs. (2.34) and (2.35)) *with eigenfunction v such that*

$$v' = a^2 u, \quad x \in [0,1], \quad \int_0^1 \frac{v}{a^2}\, ds = 0. \tag{2.39}$$

Proof. (i) Using Eq. (2.38) in Eq. (2.34), dividing by b^2 and differentiating, we obtain

$$\left(\frac{1}{b^2} u'\right)' + \lambda \frac{u}{b^2} = 0,$$

which is Eq. (2.36) for $a = b^{-1}$. Moreover, by Eq. (2.35) we have $u(0) = 0 = u(1)$ and the thesis follows. Note that if $\lambda = 0$, then $b^2 v' \equiv \text{const.}$ in $[0,1]$ and, by Eq. (2.35) $u \equiv 0$ in $[0,1]$, and u is not an eigenfunction of (Eqs. (2.36) and (2.37)).

(ii) Clearly $\lambda > 0$. By $v' = a^2 u$ in $(0,1)$ we get

$$v(x) = \int_0^x a^2 u\, ds + v(0), \quad x \in [0,1], \tag{2.40}$$

where $v(0)$ will be determined later. Note that $v'(0) = 0 = v'(1)$ by Eq. (2.37). Integrating Eq. (2.36) we obtain

$$a^2 u' + \lambda v = c \equiv \text{const.}, \qquad x \in (0,1), \tag{2.41}$$

that is

$$\left(\frac{v'}{a^2}\right)' + \lambda \frac{v}{a^2} = \frac{c}{a^2}, \quad x \in (0,1). \tag{2.42}$$

We determine now $v(0)$ such that $c = 0$. By integrating Eq. (2.42) in $(0,1)$ and recalling that $v'(0) = 0 = v'(1)$, we obtain

$$\lambda \int_0^1 \frac{v}{a^2}\, ds = c \int_0^1 \frac{ds}{a^2}. \tag{2.43}$$

Replacing the expression (Eq. (2.40)) in the left-hand side of Eq. (2.43) and imposing $c = 0$ we obtain

$$v(0) = -\frac{1}{\int_0^1 \frac{ds}{a^2(s)}} \int_0^1 \frac{1}{a^2(x)} \left(\int_0^x a^2(s) u(s)\, ds \right) dx, \tag{2.44}$$

and the proof is complete.□

We now show how to construct quasi-isospectral horns under Neumann end conditions. Consider a horn $\hat{b}$ under Neumann boundary conditions. Let $\{\lambda_m, v_m\}_{m=0}^{\infty}$ be the eigenpairs of

$$(\hat{b}^2 v')' + \lambda \hat{b}^2 v = 0, \quad x \in (0,1), \tag{2.45}$$

$$v'(0) = 0 = v'(1), \tag{2.46}$$

with $0 = \lambda_0 < \lambda_1 < \lambda_2 < \cdots$ and $\lim_{m \to \infty} \lambda_m = \infty$. By Proposition 2.1, part (i), $\{\lambda_m, u_m = \hat{b}^2 v_m'\}_{m=1}^{\infty}$ are the eigenpairs of the Dirichlet problem

$$(\hat{a}^2 v')' + \lambda \hat{a}^2 v = 0, \quad x \in (0,1), \tag{2.47}$$

$$u(0) = 0 = u(1), \tag{2.48}$$

with $\widehat{a} = \widehat{b}^{-1}$. To this point, we use the analysis of Section 2.2 to construct families of quasi-isospectral horns $a = a(x)$ (see Eq. (2.21)), that is families of cross-sectional area functions $a(x)$ such that the problem

$$(a^2 w')' + \lambda a^2 w = 0, \quad x \in (0,1), \tag{2.49}$$

$$w(0) = 0 = w(1), \tag{2.50}$$

has exactly the same eigenvalues of Eqs. (2.47) and (2.48), with the exception of the nth eigenvalue, where $n \geq 1$ is a given integer number. By Proposition 2.1, part (ii), the eigenvalues of Eqs. (2.49) and (2.50) are the positive eigenvalues of the Neumann problem

$$(b^2 y')' + \lambda b^2 y = 0, \quad x \in (0,1), \tag{2.51}$$

$$y'(0) = 0 = y'(1), \tag{2.52}$$

with $b = a^{-1}$. Note that $\lambda_0 = 0$ is the lower eigenvalue of Eqs. (2.51) and (2.52). In conclusion, the horns $\widehat{b} = \widehat{b}(x)$ and $b = b(x)$ are *Neumann quasi-isospectral*.

3. Numerical implementation of the reconstruction procedure

In order to apply the reconstruction procedure of the duct profile $a = a(x)$ based on sequential application of Eq. (2.21), a numerical code has been implemented. It is mainly based on the computation of the fundamental solutions y_1 and y_2 defined in Eqs. (2.9)–(2.11) and (2.12)–(2.14), respectively. In fact, the functions $w_{n,t}$, $\omega_{n,t}$, and z_n appearing in Eq. (2.21) can be easily calculated in terms of y_1 and y_2, for suitable values of the parameter λ. The above solutions are particular cases of the following initial value problem:

$$y'' + \lambda y = qy, \quad x \in (0,1), \tag{3.1}$$

$$y(0) = y_0, \tag{3.2}$$

$$y'(0) = \dot{y}_0, \tag{3.3}$$

where $q(x) = \frac{a''(x)}{a(x)}$, $q \in C^0([0,1])$, is the Schrödinger potential and λ is a given (real) number. To solve Eqs. (3.1)–(3.3) we have adopted the numerical integration scheme based on Stoermer's rule, see [20]. Let us introduce a grid of equally spaced points of the interval $[0,1]$, say $\{x_j\}_{j=0}^{p}$, with $x_0 = 0$, $x_j = x_0 + jH$, $j = 1, \ldots, p$ and $H = \frac{1}{p}$. At the interior points $\{x_i\}_{i=1}^{p-1}$ the potential q has been estimated by approximating the second derivative of $a(x)$ by the central finite difference formula

$$a''(x_i) \simeq \frac{a_{i-1} - 2a_i + a_{i+1}}{H^2}, \tag{3.4}$$

where $a_i = a(x_i)$ and, therefore, $q(x_i) = \frac{a''(x_i)}{a(x_i)}$. At the first and at the last point of the grid, we have set

$$a''(x_0) \simeq \frac{3a_0 - 8a_1 + 7a_2 - 2a_3}{H^2}, \tag{3.5}$$

and

$$a''(x_p) \simeq \frac{3a_p - 8a_{p-1} + 7a_{p-2} - 2a_{p-3}}{H^2}. \tag{3.6}$$

We recall that the approximations (Eqs. (3.5) and (3.6)) produce an error of order H^2 exactly as in Eq. (3.4).

Denoting by $\{y_j\}_{j=0}^{p}$ the approximation of the solution $y = y(x)$ to Eqs. (3.1)–(3.3) at the points $\{x_j\}_{j=0}^{p}$, *e.g.*, $y(x_j) \simeq y_j$, Stoermer's integration scheme is based on a further subdivision in m parts of length $h = \frac{H}{m}$ of each interval (x_j, x_{j+1}). Let us denote by $\{x_{j_k}\}_{k=0}^{m}$ the points of the sub-grid, with $x_{j_k} = x_{j_0} + kh$, $k = 0, \ldots, m$, $x_{j_0} = x_j$ and $x_{j_m} = x_{j+1}$. Moreover, let $y_{j_k} = y(x_{j_k})$. The function y at x_{j_1} is estimated by means of a parabolic extrapolation, namely

$$y_{j_1} = y_{j_0} + h\dot{y}_{j_0} + \tfrac{1}{2}h^2\left(q_{j_0} - \lambda\right)y_{j_0}, \tag{3.7}$$

where $q_{j_0} = q(x_{j_0})$. In the remaining points, the second derivative of y is estimated as

$$y''(x_{j_k}) \simeq \frac{y_{j_{k+1}} - 2y_{j_k} + y_{j_{k-1}}}{h^2} = \left(q_{j_k} - \lambda\right)y_{j_k}, \quad k = 1, \ldots, m-1. \tag{3.8}$$

At the last point, we set

$$\dot{y}_{j_m} = \frac{y_{j_m} - y_{j_{m-1}}}{h} + \frac{1}{2}h\left(q(x_{j+1}) - \lambda\right)y_{j_m}. \tag{3.9}$$

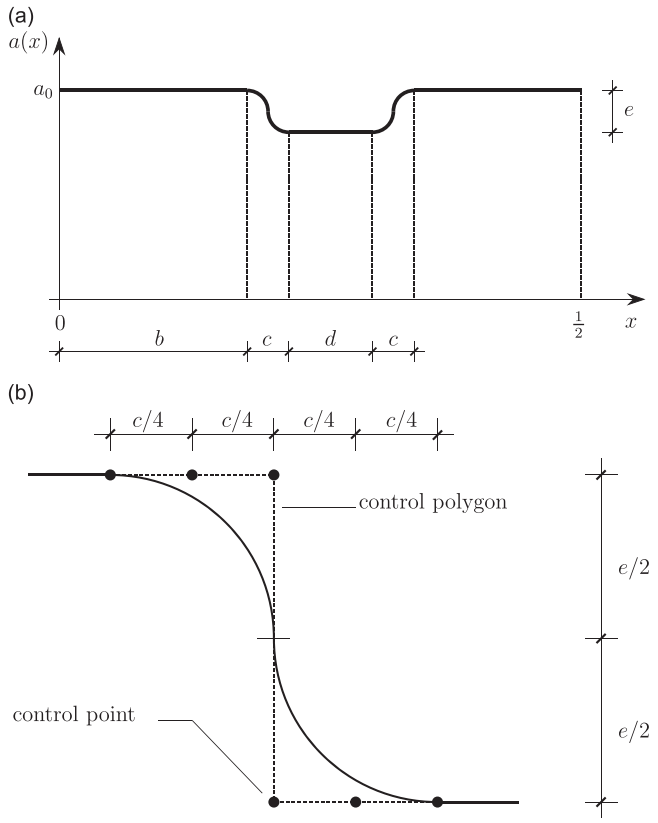

Fig. 1. Cross-sectional area function $a = a(x)$ of the symmetric duct, $a(x) = a(1-x)$ in $[0, 1]$ (a) and detail of the junction (b).

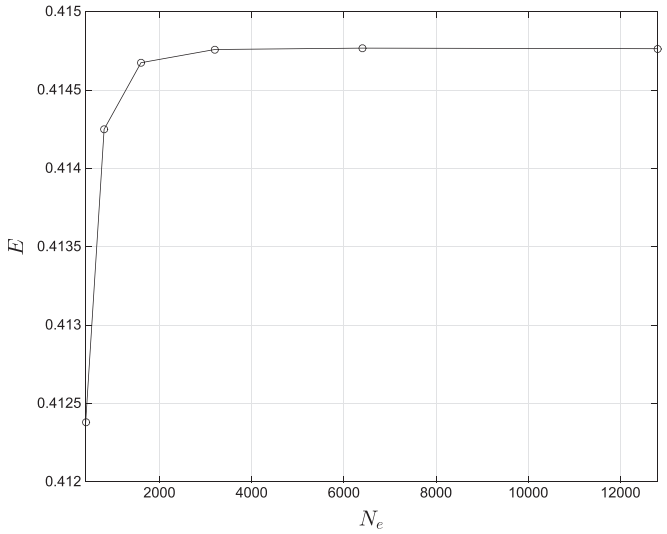

Fig. 2. Discretization error index E *vs.* number of mesh elements N_e (b=0.24, c=0.005, d=0.05, and e=0.004).

The numerical integration scheme was coded following a procedure suggested by Henrici [21], which ensures a significant roundoff error reduction. In brief, starting from

$$\Delta_0 = h\dot{y}_{j_0} + \tfrac{1}{2}h^2\left(q_{j_0} - \lambda\right)y_{j_0}, \tag{3.10}$$

$$y_{j_1} = y_{j_0} + \Delta_0, \tag{3.11}$$

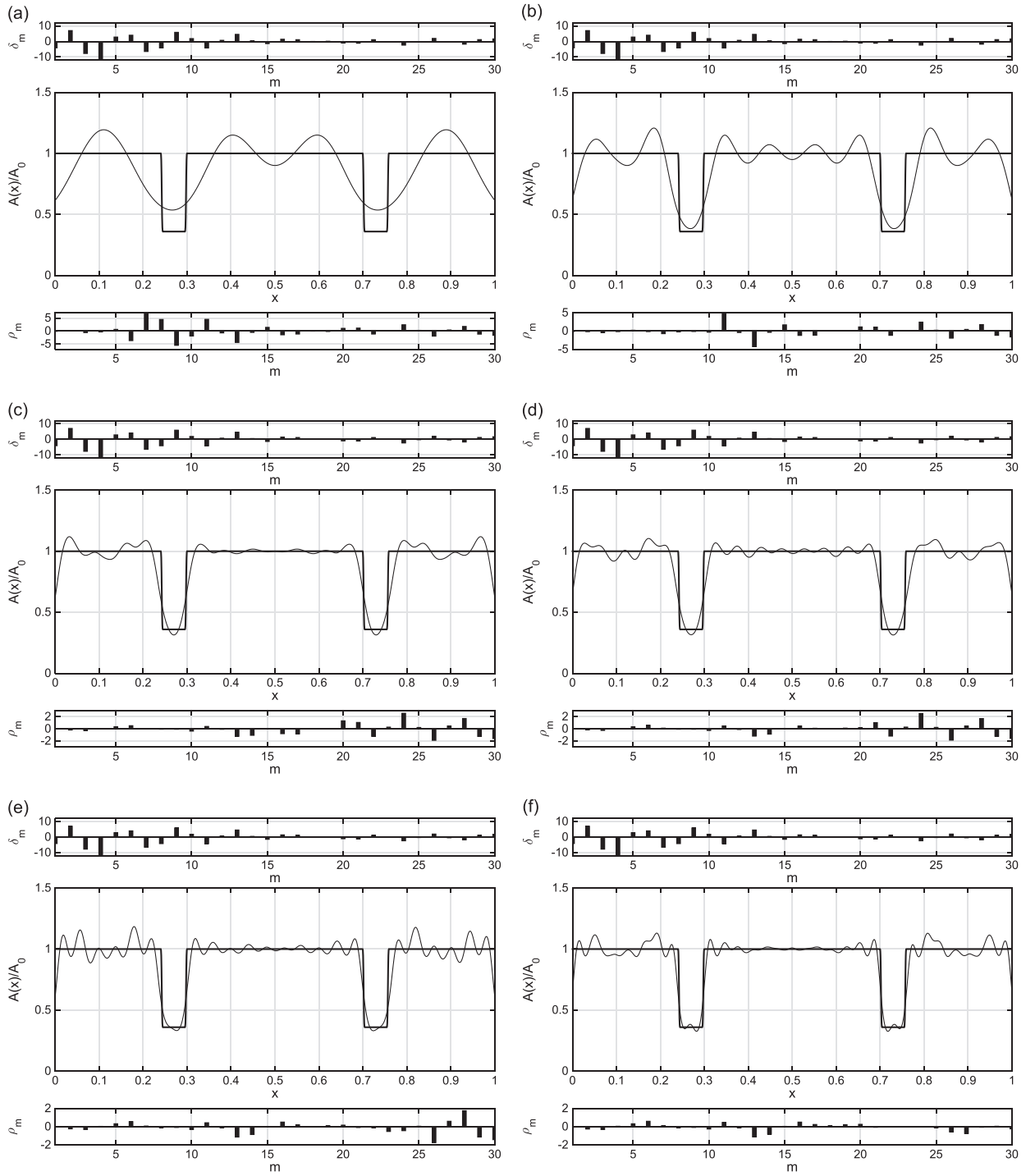

Fig. 3. Reconstruction of a duct with $b=0.24$, $c=0.005$, $d=0.05$, $e=0.004$, $N_e=1600$ ($N_e=3200$ for $N=30$ only, case (f)) using (a) $N=5$, (b) $N=10$, (c) $N=15$, (d) $N=20$, (e) $N=25$ and (f) $N=30$ first eigenfrequencies. Thick curve: exact profile; thin curve: reconstructed profile.

we evaluate the following quantities:

$$\Delta_k = \Delta_{k-1} + h^2(q_{j_k} - \lambda) y_{j_k}, \tag{3.12}$$

$$y_{j_{k+1}} = y_{j_k} + \Delta_k, \quad \text{for } k = 1, \ldots, m-1, \tag{3.13}$$

Table 1
First 30 radian frequencies of the duct without (ω_m) and with blockages (ω_{mb}). $\Delta = 100 \times (\omega_{mb}^{rec} - \omega_{mb})/\omega_{mb}$. ω_{mb} are evaluated for $N_e = 12{,}800$; ω_{mb} are evaluated using $N_e = 1600$ and $N = 20$.

Order	Radian frequency			Δ
	ω_m	ω_{mb}	ω_{mb}^{rec}	
1	3.1416	3.0107	3.0101	−0.02
2	6.2832	6.7248	6.7146	−0.15
3	9.4248	8.6937	8.6708	−0.26
4	12.5664	11.0619	11.0686	0.06
5	15.7080	16.1593	16.2184	0.37
6	18.8496	19.6163	19.7347	0.60
7	21.9911	20.5655	20.5930	0.13
8	25.1327	24.0772	24.0617	−0.06
9	28.2743	29.9456	29.9254	−0.07
10	31.4159	32.0077	31.9216	−0.27
11	34.5575	33.0911	33.2568	0.50
12	37.6991	37.9925	37.9530	−0.10
13	40.8407	42.7266	42.2157	−1.20
14	43.9823	44.2124	43.8278	−0.87
15	47.1239	46.4577	46.5010	0.09
16	50.2655	51.0123	51.2582	0.48
17	53.4071	54.0402	54.1037	0.12
18	56.5487	56.5754	56.5760	0.00
19	59.6903	59.8039	59.8864	0.14
20	62.8319	62.1715	62.3064	0.22
21	65.9734	65.2124	65.8915	1.04
22	69.1150	69.9346	69.1003	−1.19
23	72.2566	72.2114	72.4317	0.31
24	75.3982	73.6017	75.4788	2.55
25	78.5398	78.3099	78.5107	0.26
26	81.6814	83.3244	81.7777	−1.86
27	84.8230	84.4511	84.8588	0.48
28	87.9646	86.4121	87.8917	1.71
29	91.1062	92.2168	91.0939	−1.22
30	94.2478	95.8300	94.3116	−1.58

and, finally, we determine

$$\dot{y}_{j_m} = \frac{\Delta_{m-1}}{h} + \frac{1}{2} h (q(x_0 + H) - \lambda) y_{j_m}. \tag{3.14}$$

It is suggested to take an even value of m in order to improve numerical efficiency, see [20,22]. In our code we have used $m = 2$.

In order to check the accuracy of the reconstruction and to provide input data in our simulations, a numerical procedure for solving the eigenvalue problem (Eqs. (2.1) and (2.2)) was also implemented. The weak formulation of the eigenvalue problem (Eqs. (2.1) and (2.2)) (with $\widehat{A}(x)$ replaced by $A(x)$) consists in finding $u \in H_0^1(0,1) \setminus \{0\}$ and $\lambda \in \mathbb{R}$ such that

$$\int_0^1 A u' \varphi' = \lambda \int_0^1 A u \varphi, \quad \text{for every } \varphi \in H_0^1(0,1). \tag{3.15}$$

Here, $H_0^1(0,1)$ is the Hilbert space of Lebesgue measurable functions $f: (0,1) \to \mathbb{R}$ such that f and its first weak derivative f' are square integrable in $(0,1)$, *e.g.* $\| f \|^2_{H^1(0,1)} = \int_0^1 (f^2 + (f')^2) < \infty$, and the trace of f at $x = 0$ and $x = 1$ vanishes, *e.g.*, $f(0) = f(1) = 0$. To find a discrete version of Eq. (3.15), we work on the finite dimensional subspace $\mathcal{H}$ of the second-order B-spline test functions [23]. These test functions allow us to obtain very refined results with computational cost similar to that of piecewise constant interpolation, see, for example, [24,25] for second-order B-spline interpolation in finite element analysis for two- and three-dimensional problems. The one-dimensional case used here can be easily derived from [26,27]. The expressions of the three test functions on the generic eth finite element (coinciding with the normalized interval $(-1, 1)$) are

$$\Phi_e = \begin{bmatrix} \frac{1}{8}\left(1 - 2\xi + \xi^2\right) \\ \frac{1}{4}\left(3 - \xi^2\right) \\ \frac{1}{8}\left(1 + 2\xi + \xi^2\right) \end{bmatrix}, \tag{3.16}$$

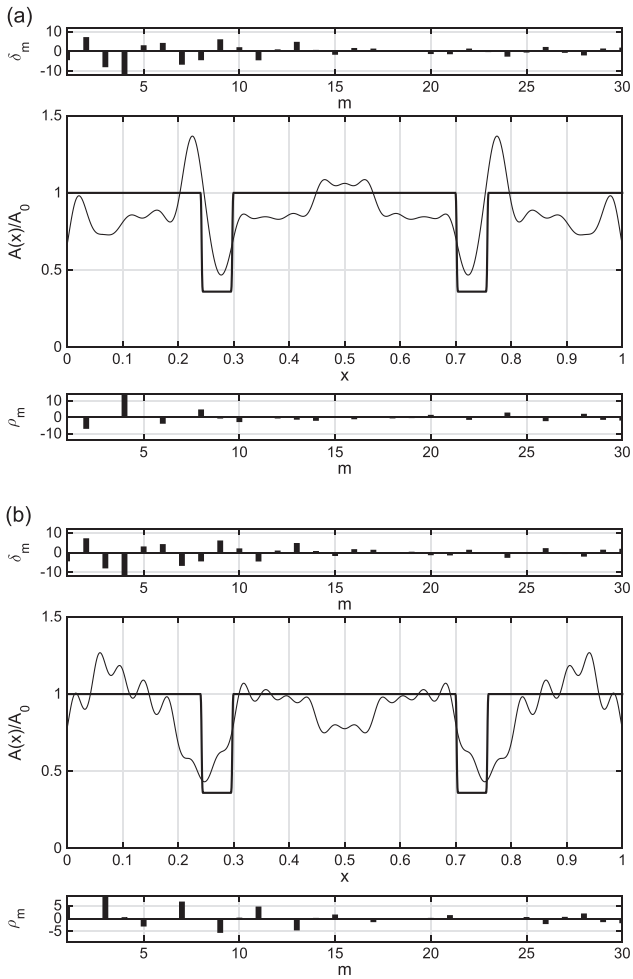

Fig. 4. Reconstruction of the duct as in Fig. 3 for $N=25$, and using the first odd (a) and the first even (b) eigenfrequencies only. Thick curve: exact profile; thin curve: reconstructed profile.

whereas the expressions corresponding to the first (near $x=0$) and the last (near $x=1$) finite element are

$$\Phi_1 = \begin{bmatrix} \frac{1}{4}\left(1-2\xi+\xi^2\right) \\ \frac{1}{8}\left(5+2\xi-3\xi^2\right) \\ \frac{1}{8}\left(1+2\xi+\xi^2\right) \end{bmatrix}, \quad \Phi_n = \begin{bmatrix} \frac{1}{8}\left(1-2\xi+\xi^2\right) \\ \frac{1}{8}\left(5-2\xi-3\xi^2\right) \\ \frac{1}{4}\left(1+2\xi+\xi^2\right) \end{bmatrix}. \tag{3.17}$$

On each finite element we use the approximation $\tilde{u}_e$ of u given by

$$\tilde{u}_e \simeq \mathbf{\Phi}_e^T \mathbf{u}_e, \tag{3.18}$$

where $\mathbf{\Phi}_e^T$ is the row vector containing the test functions and $\mathbf{u}_e$ is the vector of the unknowns. Replacing Eq. (3.18) in Eq. (3.15), the discrete version of Eq. (3.15) consists in solving the finite dimensional eigenvalue problem

$$\mathbf{K}\tilde{\mathbf{u}} = \tilde{\lambda}\mathbf{M}\tilde{\mathbf{u}}, \tag{3.19}$$

where $(\tilde{\lambda}, \tilde{\mathbf{u}})$ is the approximation of the continuous eigenpair (λ, u). The stiffness and inertia matrices $\mathbf{K}$ and $\mathbf{M}$ are obtained by means of a standard finite element procedure of assemblage of the local matrices $\mathbf{K}_e$ and $\mathbf{M}_e$, which are defined as

$$\mathbf{K}_e = \int_{-1}^{1} A\, \mathbf{\Phi}_e' \mathbf{\Phi}_e'^T J \, \mathrm{d}\xi, \quad \mathbf{M}_e = \int_{-1}^{1} A \mathbf{\Phi}_e \mathbf{\Phi}_e^T J \, \mathrm{d}\xi. \tag{3.20}$$

Here, the Jacobian J links the normalized and physical eth finite element. The numerical integration in Eq. (3.20) was

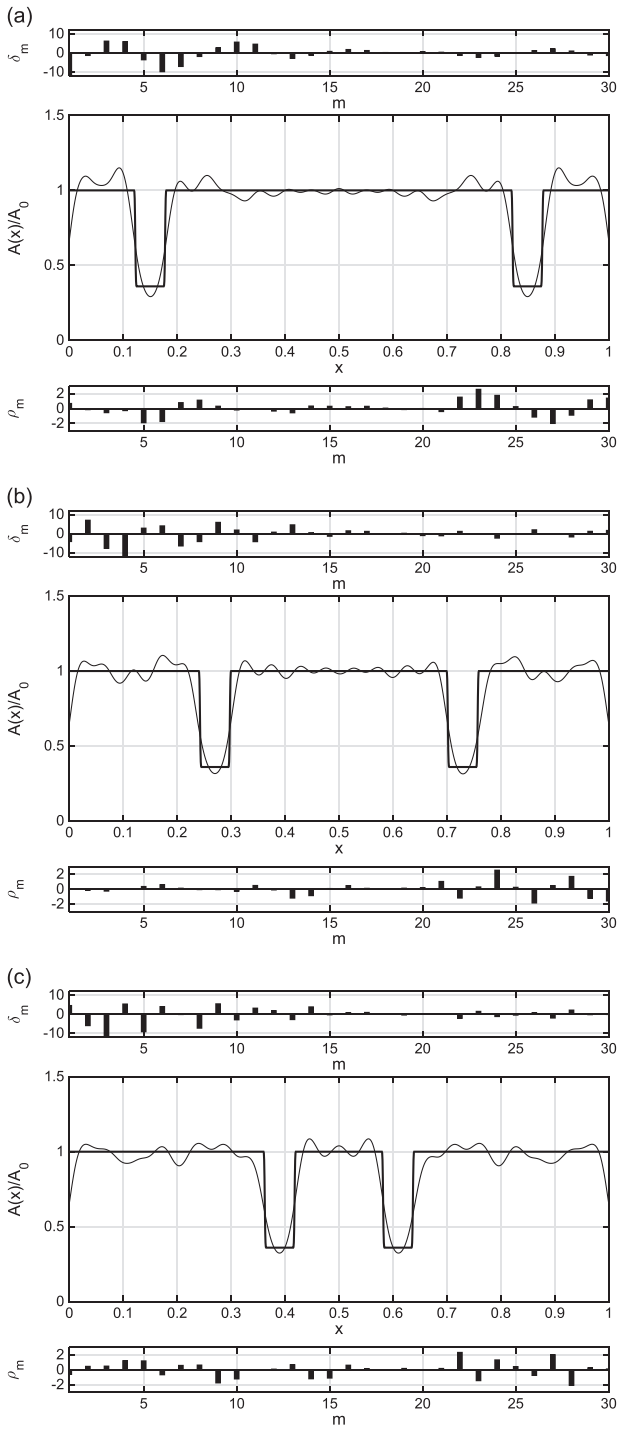

Fig. 5. Reconstruction of a duct with $c=0.005$, $d=0.05$, and $e=0.004$, varying the position b; $N=20$, $N_e=1600$. (a) $b=0.12$; (b) $b=0.24$; and (c) $b=0.36$. Thick curve: exact profile; thin curve: reconstructed profile.

performed by using Gaussian quadrature procedure with 8 points, which produces exact results for polynomials up to degree 15.

We conclude by noticing that after each application of Eq. (2.21), the duct profile $A=A(x)$ was multiplied by a suitable positive constant such that $\int_0^1 A^{-1}(x)\,dx$ takes the prescribed value. No difference was noticed in the results of the reconstruction by prescribing the average value of the unknown coefficient (*e.g.*, $\int_0^1 A(x)\,dx$) instead of the average of the inverse of $A(x)$.

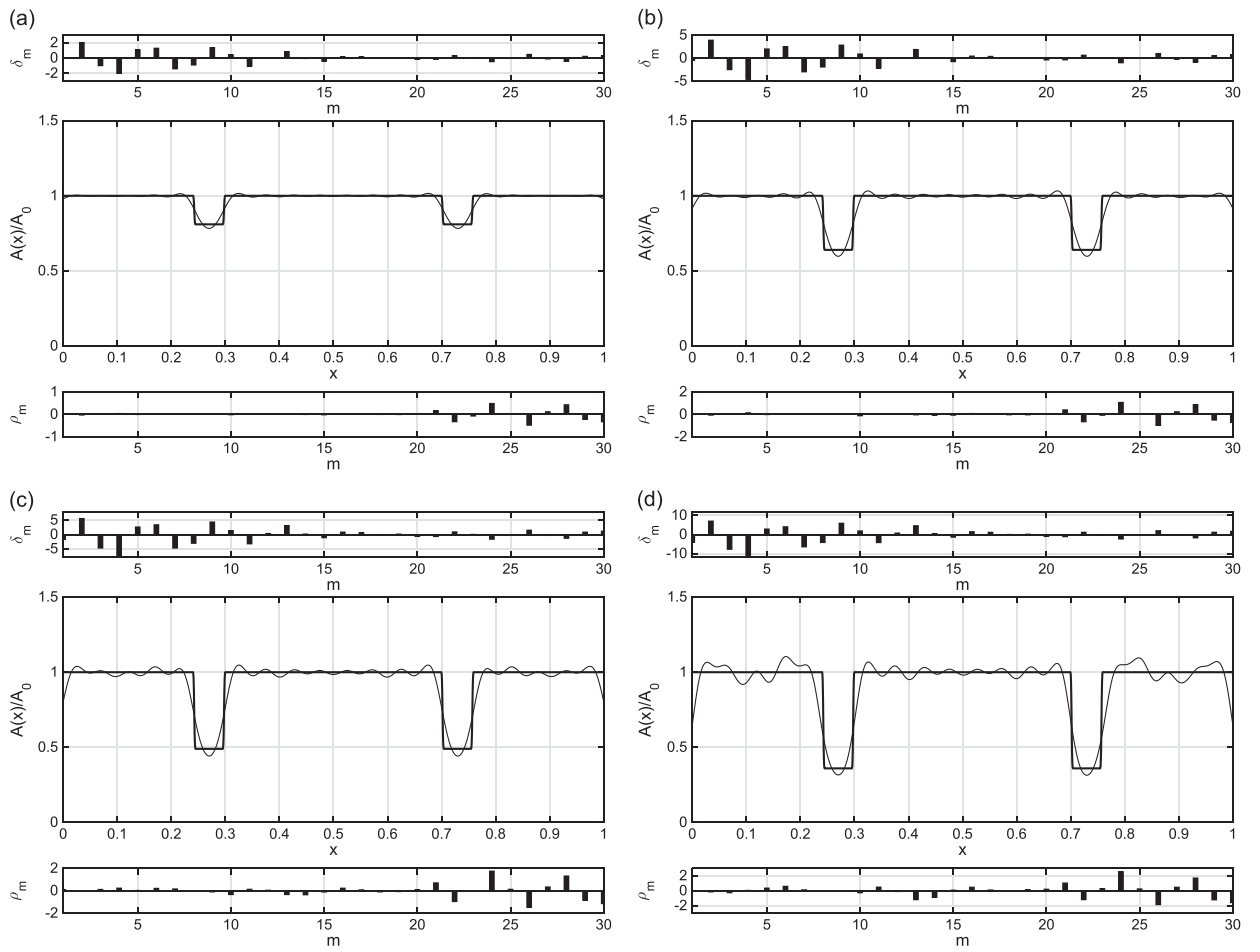

Fig. 6. Reconstruction of a duct with $b=0.24$, $c=0.005$, and $d=0.05$, varying the depth e; $N=20$, $N_e=1600$. (a) $e=0.001$; (b) $e=0.002$; (c) $e=0.003$; and (d) $e=0.004$. Thick curve: exact profile; thin curve: reconstructed profile.

4. Numerical experiments and results

In this section we shall present some results of the numerical implementation of the procedure illustrated in Section 2.3 for an open–open duct with smooth symmetric profile. An extensive numerical study was conducted to assess the stability of the reconstruction with respect to the number of eigenfrequencies used (Section 4.3); the blockage profile (Section 4.4); and the order chosen in assigning the eigenfrequencies (Section 4.6). The case of closed–closed end conditions is considered in Section 4.7. Section 4.8 deals with the influence of errors on the data. An application of the method to the detection of not symmetrical blockages is discussed in Section 4.9.

4.1. Blockage modelling

Among several simulations, we shall present a selected, but representative, set of results which refer to the specimen shown in Fig. 1(a). The unperturbed duct is a cylinder having circular cross-section of area $A_0 = a_0^2$, with $a_0=0.01$, and length $L=1$. The perturbed duct is assumed to have axially symmetric shape with circular cross-section of area $A(x) = a^2(x)$, $a^2(x) = a^2(1-x)$ in $[0, 1]$. The typical blockage profile is designed as a fifth-order Bézier curve with 6 control points, see Fig. 1 (b), in such a way to satisfy C^2-continuity of the coefficient $a(x)$ in $[0, 1]$. For a depth discussion on mathematical properties of Bézier curves we refer to the book [23], see also [28] for an application of NURBS – that are a generalization of Bézier curves – in one-dimension. We recall that a fifth-order Bézier curve is defined as

$$\mathbf{C}_5(\xi) = \sum_{i=0}^{5} B_{i,5}(\xi)\mathbf{P}_i, \quad 0 \le \xi \le 1, \tag{4.1}$$

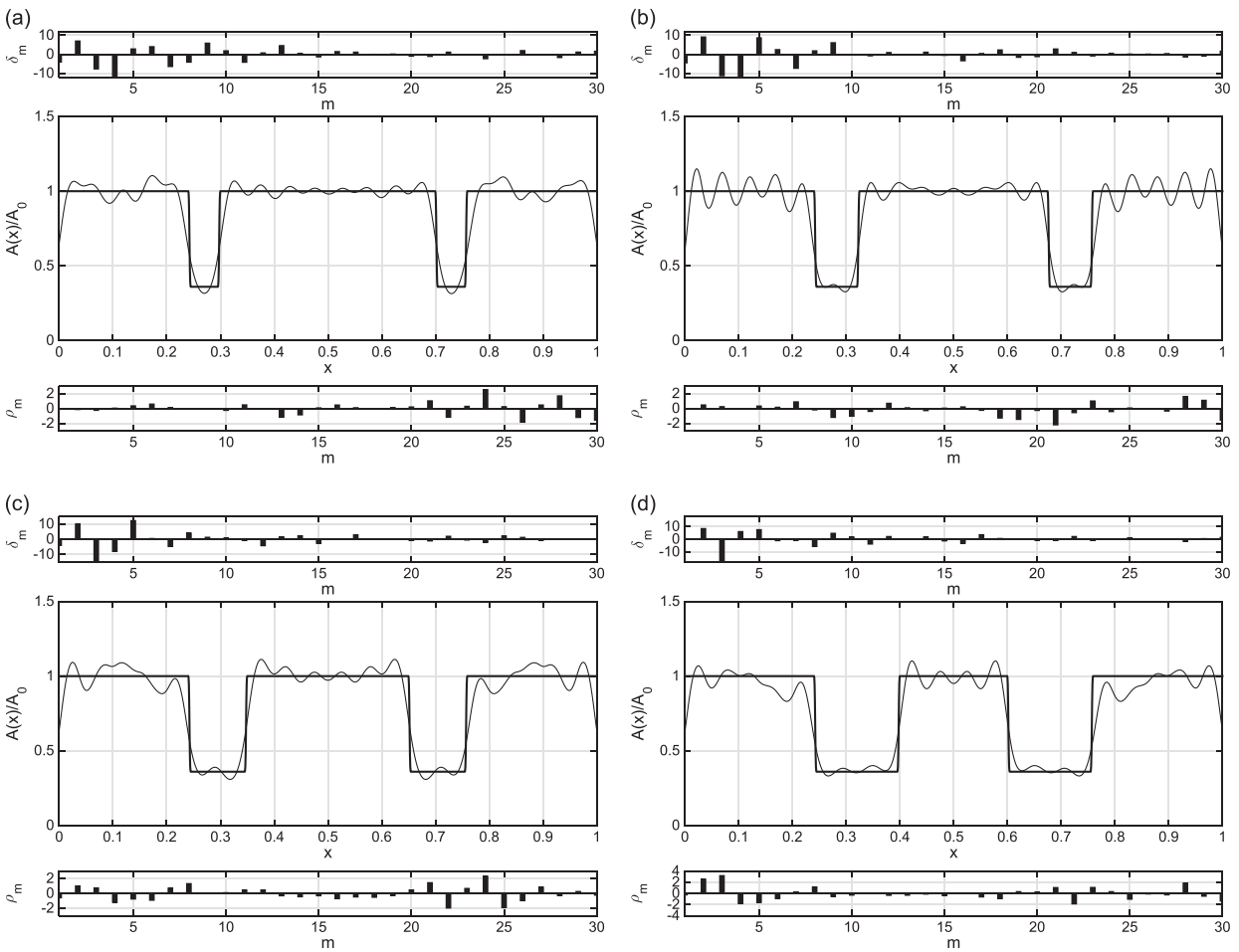

Fig. 7. Reconstruction of a duct with $b=0.24$, $c=0.005$, and $e=0.004$, varying the width d; $N=20$, $N_e=1600$. (a) $d=0.05$; (b) $d=0.075$; (c) $d=0.1$; and (d) $d=0.15$. Thick curve: exact profile; thin curve: reconstructed profile.

where $B_{i,5}(\xi)$ are the fifth-degree blending functions, *i.e.*, the fifth-degree Bernstein's polynomials, and $\mathbf{P}_i$ the control points. The explicit formulae for the blending functions are

$$\begin{aligned} B_{0,5} &= (1-\xi)^5, \\ B_{1,5} &= 5\xi(1-\xi)^4, \\ B_{2,5} &= 10\xi^2(1-\xi)^3, \\ B_{3,5} &= 10\xi^3(1-\xi)^2, \\ B_{4,5} &= 5\xi^4(1-\xi), \\ B_{5,5} &= \xi^5. \end{aligned} \tag{4.2}$$

Control points used to model the left junctions, see Fig. 1, are defined by

$$\begin{aligned} \mathbf{P}_0 &= (b, a_0), \\ \mathbf{P}_1 &= \left(b+\tfrac{1}{4}c, a_0\right), \\ \mathbf{P}_2 &= \left(b+\tfrac{1}{2}c, a_0\right), \\ \mathbf{P}_3 &= \left(b+\tfrac{1}{2}c, a_0-e\right), \\ \mathbf{P}_4 &= \left(b+\tfrac{3}{4}c, a_0-e\right), \\ \mathbf{P}_5 &= (b+c, a_0-e), \end{aligned} \tag{4.3}$$

while for the right junction we set

$$\begin{aligned} \mathbf{P}_0 &= (b+c+d, a_0-e), \\ \mathbf{P}_1 &= \left(b+c+d+\tfrac{1}{4}c, a_0-e\right), \end{aligned}$$

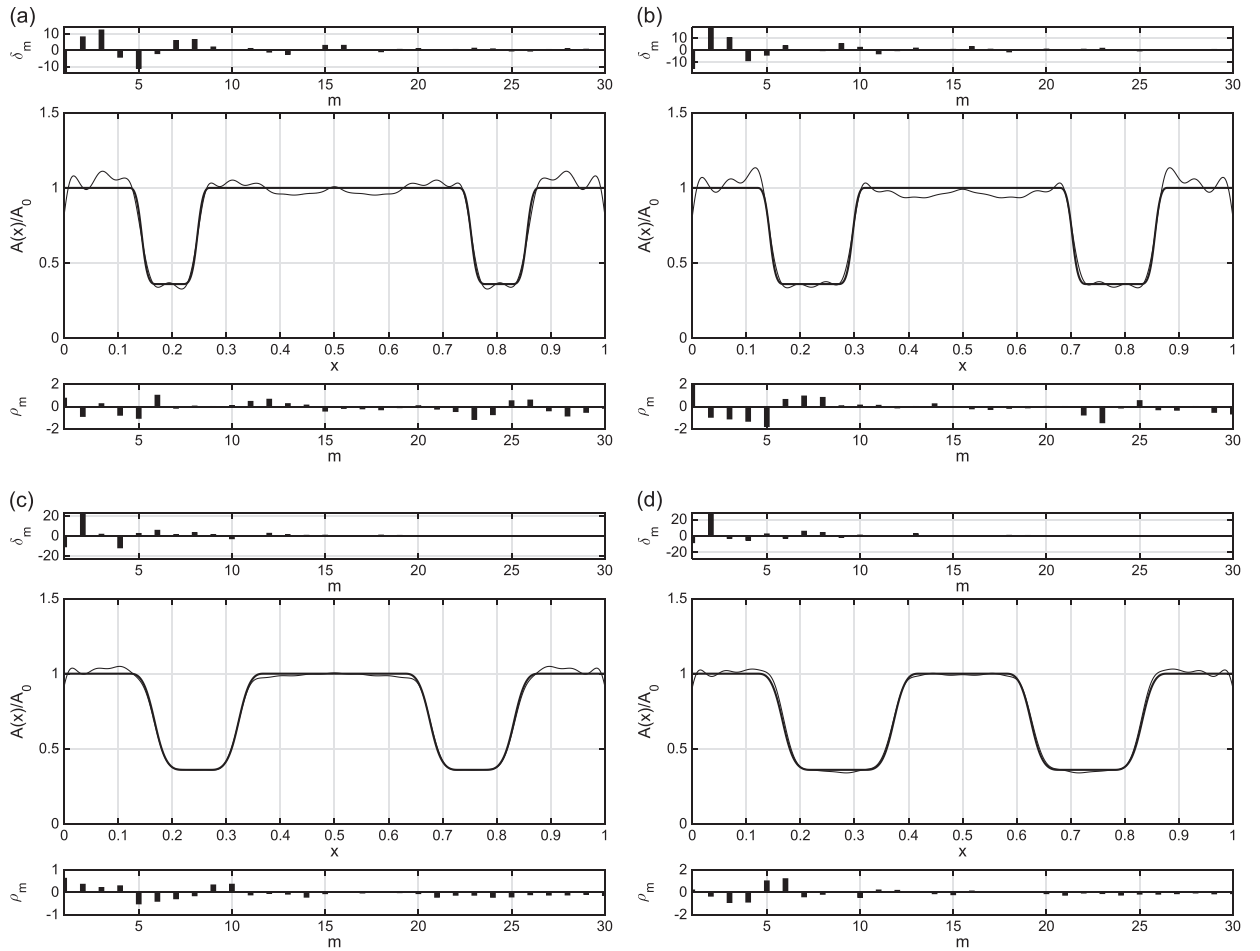

Fig. 8. Reconstruction of a duct with $b=0.12$ and $e=0.004$, varying the joint length c and the width d; $N=20$, $N_e=1600$. (a) $c=0.05$ and $d=0.05$; (b) $c=0.05$ and $d=0.1$; (c) $c=0.1$ and $d=0.05$; and (d) $c=0.1$ and $d=0.1$. Thick curve: exact profile; thin curve: reconstructed profile.

$$\begin{aligned}\mathbf{P}_2 &= \left(b+c+d+\tfrac{1}{2}c, a_0-e\right),\\ \mathbf{P}_3 &= \left(b+c+d+\tfrac{1}{2}c, a_0\right),\\ \mathbf{P}_4 &= \left(b+c+d+\tfrac{3}{4}c, a_0\right),\\ \mathbf{P}_5 &= (b+c+d+c, a_0).\end{aligned} \tag{4.4}$$

All the simulations have been performed by assuming a unitary value of the sound velocity.

4.2. The finite element mesh size

In order to rationally select the finite element mesh, we first study the unperturbed horn. In this case, the exact eigenvalues values $\lambda_m = m^2\pi^2$, $m \geq 1$, can be used to compute the numerical error produced by the discrete approximation of the problem. It is possible to show that percentage discrepancy on the first 25 eigenvalues is at most 0.06 percent of the theoretical value for a mesh of $N_e=100$ equally spaced finite elements. Fig. 2 reports the discretization error index

$$E_{N_e} = \sqrt{\sum_{m=1}^{p}\left(\frac{\Delta\lambda_m}{\lambda_m}\right)^2} \tag{4.5}$$

for a duct with blockages defined by $b=0.24$, $c=0.005$, $d=0.05$, $e=0.004$ for $N_e=400$, 800, 1600, 3200, 6400, 12,800. In Eq. (4.5), $\Delta\lambda_m$ is the difference between the numerical and theoretical values of the mth eigenvalue. The plot, referred to the case $p=25$, clearly shows that numerical estimates obtained for $N_e=12{,}800$ are very accurate. However, the plot also shows that the error indicator $E_{N_e=1600}$ differs approximatively by 0.02 percent with respect to $E_{N_e=12{,}800}$, revealing that the $N_e=1600$ element mesh is a good compromise between accuracy and computational cost.

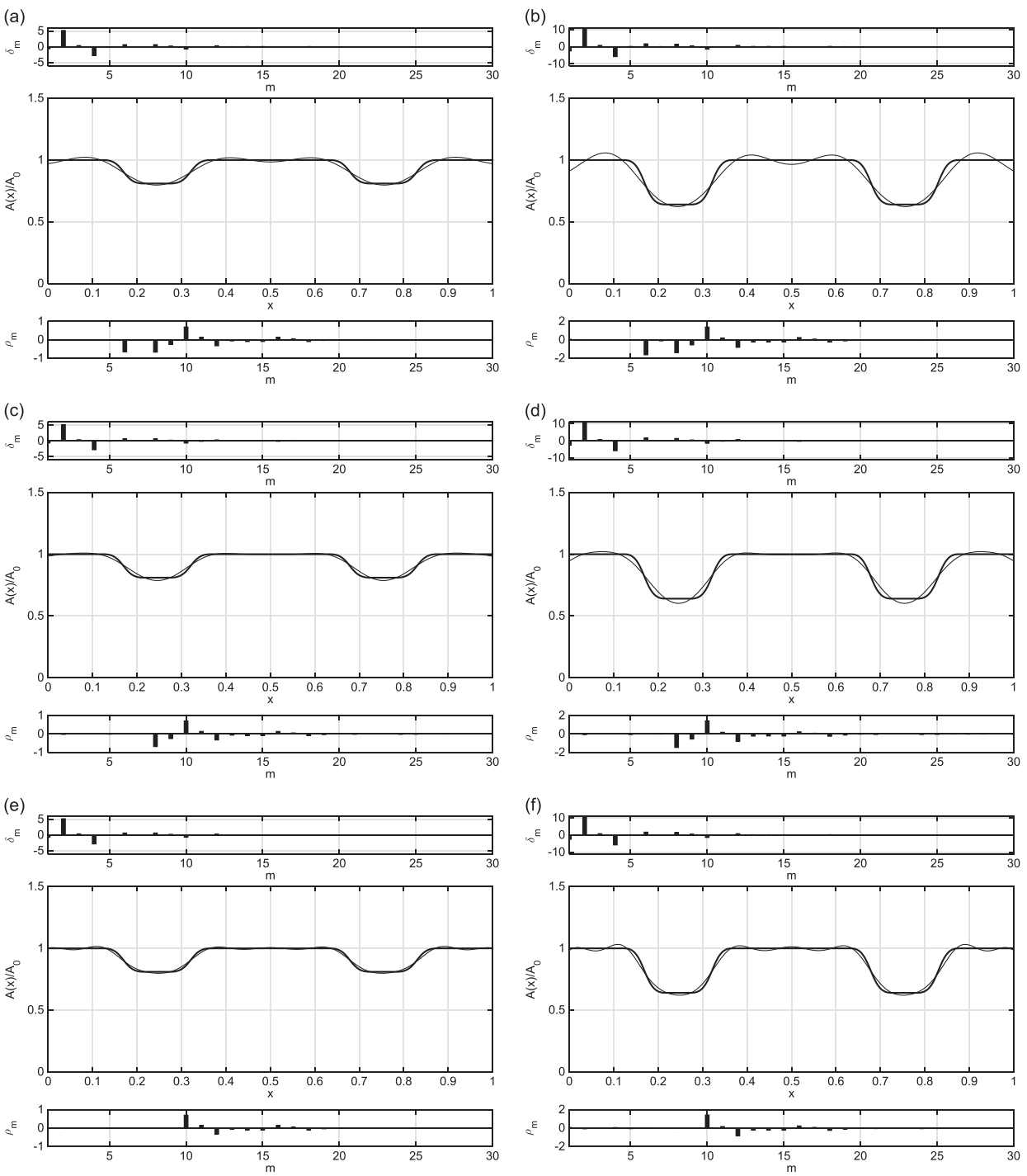

Fig. 9. Reconstruction of a duct with $b=0.12$, $c=0.1$, $d=0.05$, $N_e=1600$; $e=0.001$ in (a), (c), (e) and $e=0.002$ in (b), (d), (f). (a, b) $N=5$; (c, d) $N=7$; and (e, f) $N=9$. Thick curve: exact profile; thin curve: reconstructed profile.

4.3. The number of measured eigenfrequencies

The influence of the number N of given eigenfrequencies on the reconstruction results is analyzed in this section. Among a large number of simulations, we have chosen to test the identification technique on the most challenging and difficult cases which, in our experience, correspond to rather abrupt change of cross-sectional area concentrated on a small interval

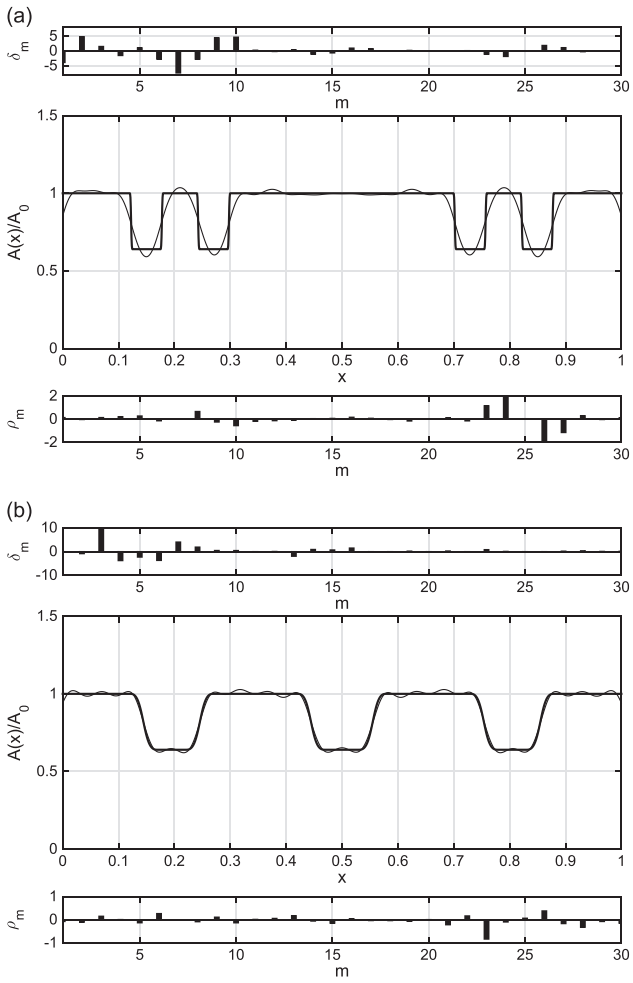

Fig. 10. Reconstruction of multiple blockages in a half of the duct. Geometrical characteristics of each blockage: (a) $b=0.12$, $c=0.005$, $d=0.05$, $e=0.002$ and (b) $b=0.12$, $c=0.05$, $d=0.05$, $e=0.002$; the distance between two adjacent blockages is $2c+d$; $N=20$, $N_e=1600$. Thick curve: exact profile; thin curve: reconstructed profile.

of the duct axis (c and d small, and e large). In particular, reference is made to the blockage parameters $b=0.24$, $c=0.005$, $d=0.05$, $e=0.004$, and the target frequency values are assigned in ascending order. For these cases, in spite of the abrupt changes, the Webster model was assumed to hold. Fig. 3 shows the results using the first 5, 10, 15, 20, 25 and 30 eigenfrequencies. Thick and thin curves represent the exact and the reconstructed profile, respectively. At the top of each subfigure, the eigenfrequency percentage shifts δ_m induced by the blockage on the uniform duct are represented, *e.g.*, $\delta_m = 100 \times (\omega_m^{\text{block}} - \omega_m^{\text{unif}})/\omega_m^{\text{unif}}$, $m = 1, \ldots, 30$. The differences ρ_m between computed (after the reconstruction) and target eigenfrequency values are shown on the bottom, *e.g.*, $\rho_m = 100 \times (\omega_m^{\text{rec}} - \omega_m^{\text{target}})/\omega_m^{\text{target}}$, $m = 1, \ldots, 30$. It can be noticed that the accuracy of the reconstruction improves as the number of eigendata increases, and the reconstructed coefficient is a good approximation of the exact profile when the first 20 frequencies are considered as input data. It should be also remarked that the eigenfrequencies of the reconstructed profile are almost coincident with the target values.

All the above simulations refer to a $N_e=1600$ mesh, with the exception of the case $N=30$ (Fig. 3(f)). It can be shown that this case requires at least 3200 elements to prevent numerical instability. In all the remaining cases, no improvement was noticed by refining (*e.g.*, halving) the mesh size in blockage reconstruction. Table 1 collects the first 30 frequencies of the duct without/with blockages and the corresponding frequencies of the reconstructed duct, with $N_e=1600$ and $N=20$. The last column on the right end side of the table collects the percentage differences between the target and the numerical values of the eigenfrequencies evaluated for the reconstructed profile.

Besides the number of eigendata, numerical simulations show that the reconstruction is significantly influenced by the set of eigendata used. For the same duct profile considered in Fig. 3, Fig. 4 shows the results obtained by taking $N=25$ and using the odd (Fig. 4(a), thirteen frequencies) and the even (Fig. 4(b), twelve frequencies) data only. A comparison with Fig. 3(b)

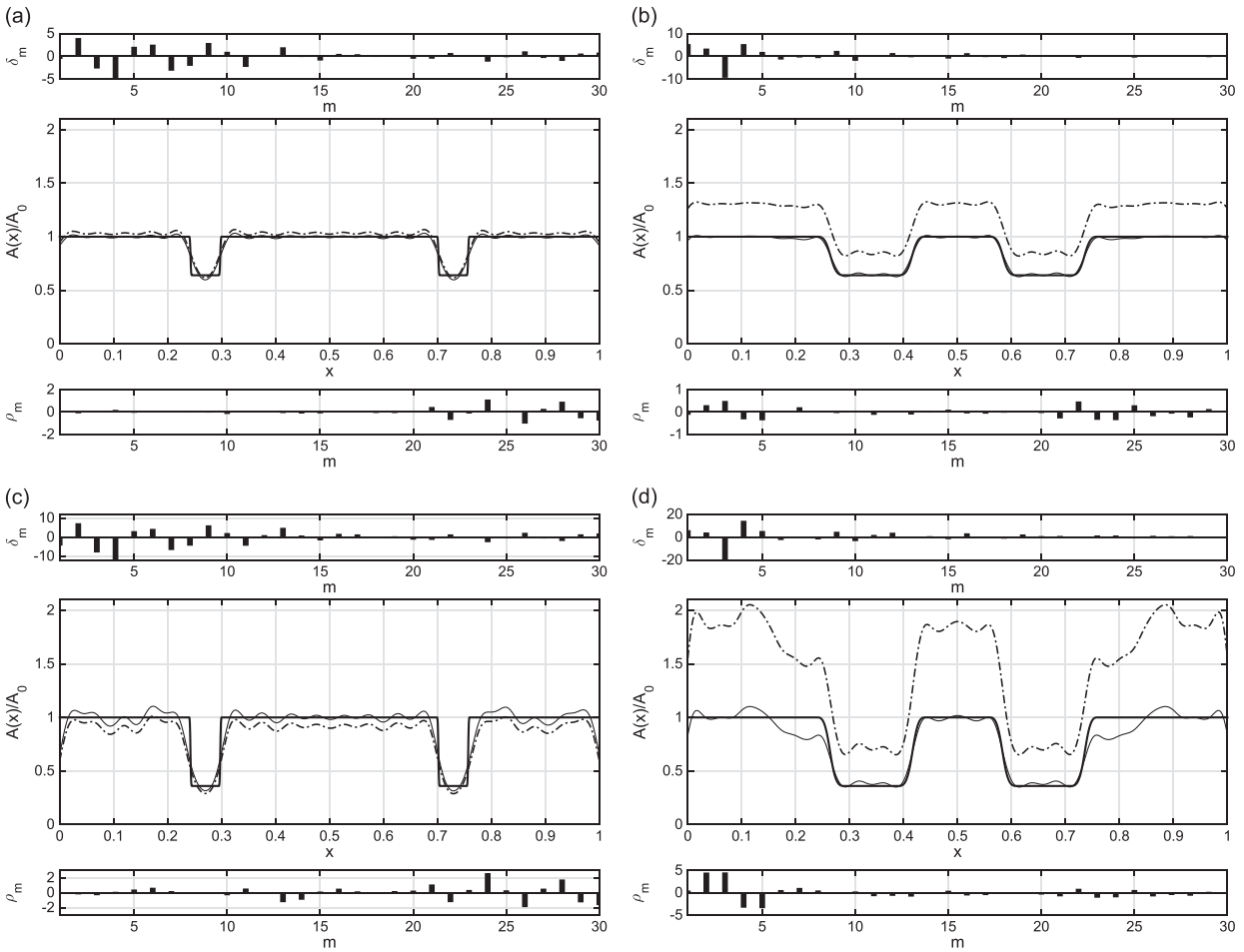

Fig. 11. Reconstruction of a duct with $b=0.24$ for $N=20$ and $N_e=1600$, by including (thin line) and excluding (dash-dotted line) the scalar information $\int_0^1 A^{-1}(x)\,dx$. (a) $c=0.005$, $d=0.05$ and $e=0.002$; (b) $c=0.05$, $d=0.1$ and $e=0.002$; (c) $c=0.005$, $d=0.05$ and $e=0.004$; and (d) $c=0.05$, $d=0.1$ and $e=0.004$. Thick curve: exact profile; thin curve: reconstructed profile.

($N=10$) and Fig. 3(c) ($N=15$) confirms that the results depend appreciably on this choice, and that – on assuming the same number of input data – better reconstruction is obtained by including both even and odd frequencies in the analysis.

4.4. Influence of the blockage profile

The reconstruction algorithm has been tested on different blockage scenarios. All the results presented in this section are obtained for $N_e=1600$ and, with the exception of Figs. 8 and 9 for $c=0.005$ and $N=20$.

Fig. 5 reports the blockage identification for $d=0.05$, $e=0.004$ and varying the position b. The influence of the depth e is analyzed in Fig. 6, for a given position $b=0.24$ of the blockage. We notice that $e=0.001$ corresponds to a reduction of the cross-sectional area of 19 percent, whereas the case $e=0.004$ corresponds to an area reduction equal to 64 percent. Fig. 7 collects the results obtained by varying the width d of the blockage, for $b=0.24$ and $e=0.004$. Finally, the effect of changing the joint length c and the width d is shown in Figs. 8 and 9. The cases studied refer to $b=0.12$. Comparing Figs. 8 and 9 it clearly emerges that, for a given number of first frequencies, the accuracy of the reconstruction increases for diffuse and smooth blockages, that is when both c and d are larger. This feature of the reconstruction method could be of importance in practical applications, since experimental results obtained in real ducts with diffuse blockages show that Webster model is more accurate in the range of low frequencies, see, for example, [15].

The reconstruction method has been also tested in case of multiple blockages in one-half of the duct. Fig. 10(a) reports the identification of two blockages, with $b=0.12$, $c=0.005$, $d=0.05$ and $e=0.002$. The distance between two neighboring blockages is assumed as $2c+d$. The results shown in Fig. 10(b) refer to a symmetric duct profile with two lateral blockages and a third blockage whose support is centered at the mid-point $x=\frac{1}{2}$, for $b=0.12$, $c=0.05$, $d=0.05$ ($d=0.06$ for the central blockage) and $e=0.002$. Also in this case the distance between two adjacent blockages is $2c+d$.

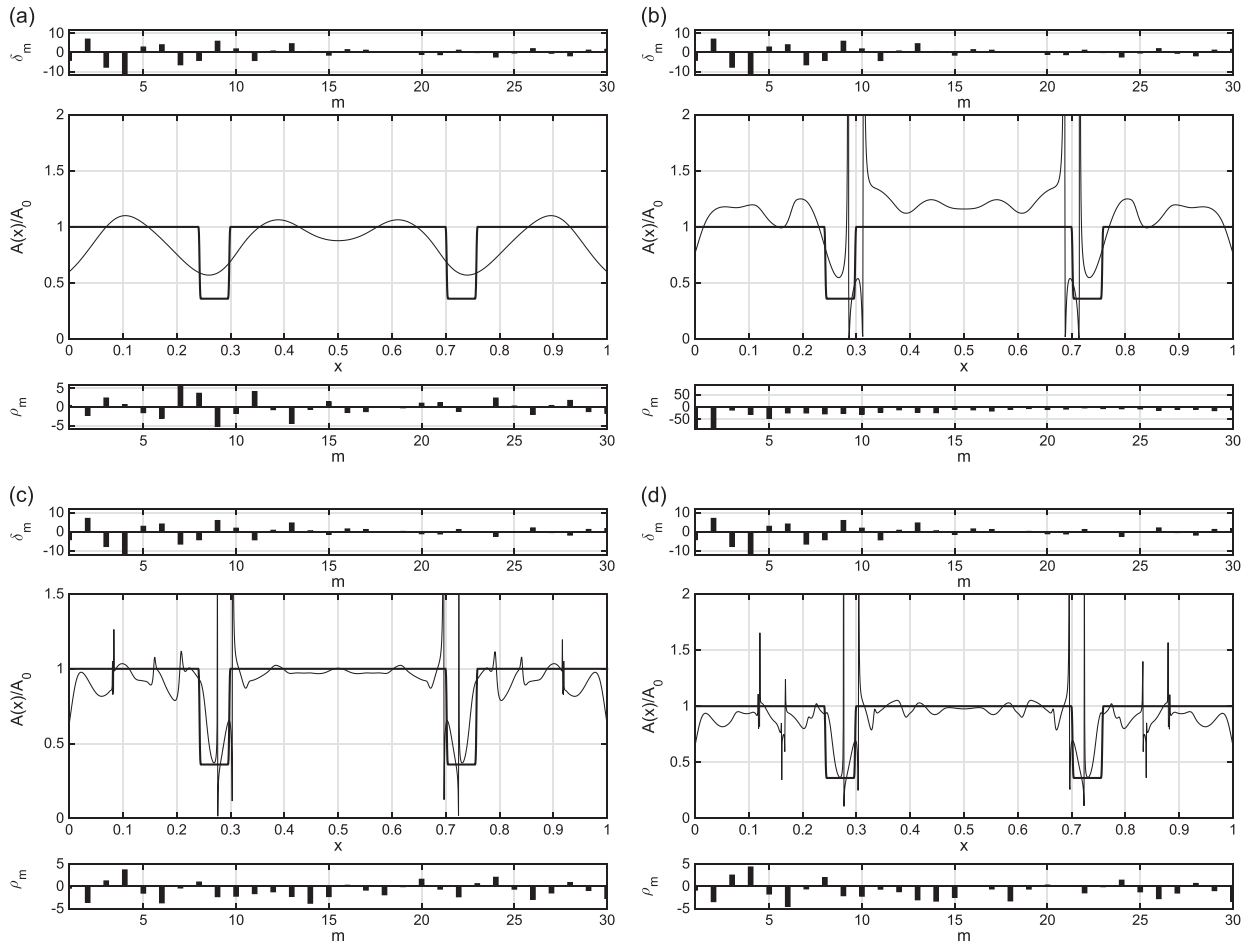

Fig. 12. Reconstruction of the duct as in Fig. 3 ($N_e=1600$) using (a) $N=5$, (b) $N=10$, (c) $N=15$ and (d) $N=20$ first eigenfrequencies in reverse order. Thick curve: exact profile; thin curve: reconstructed profile.

Generally speaking, the reconstruction is in good agreement with the exact coefficient in all the cases considered, suggesting that the method is rather stable to different blockage profiles.

4.5. Scaling effect

It has been noticed at the end of Section 2.3 that, even when all the eigenfrequencies are given, the unique reconstruction of the duct profile requires an additional scalar information on the coefficient $A(x)$. In our analysis, this information coincides with $\int_0^1 A^{-1}(x)\,dx$. Fig. 11 compares the results obtained with and without including this information on the spectral data. The results refer to $N_e=1600$, $N=20$, $b=0.24$ and $e=0.04$. Numerical results confirm that the scaling parameters strongly influence the accuracy of the reconstruction, especially in the case of large blockages, see also [13].

4.6. The order of assigning the measured eigenfrequencies

All the previous results have been obtained by assigning the first N frequencies in ascending order, *i.e.*, from the first to the Nth. In this section we shall investigate the effect of assigning the target values in descending order. With reference to the blockage profile considered in Section 4.3 and for $N_e=1600$, Fig. 12 shows the reconstruction obtained with $N=5, 10, 15, 20$. In spite of the equivalence of the reconstruction procedure expected from the theory, numerical simulations show an appreciable deterioration of the results, with the appearance of numerical instabilities and large oscillations around the exact profile. A refinement of the finite element mesh was not useful in these cases.

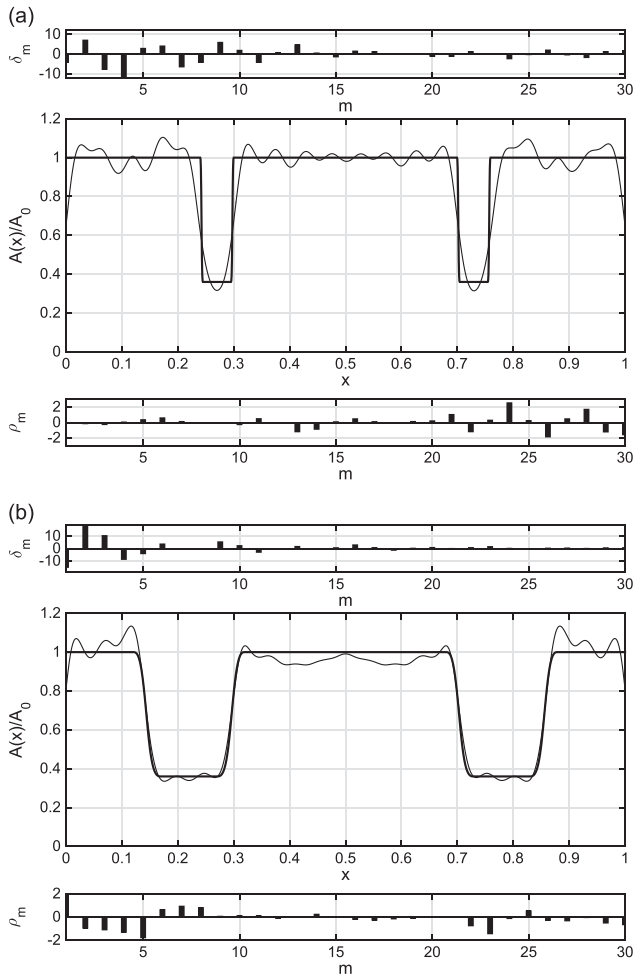

Fig. 13. Reconstruction of a duct under closed–closed end conditions, with (a) $b=0.24$, $c=0.005$, $d=0.05$, $e=0.004$ and (b) $b=0.12$, $c=0.05$, $d=0.1$, $e=0.004$; $N=20$ (ascending order), $N_e=1600$. Thick curve: exact profile; thin curve: reconstructed profile.

4.7. Closed–closed end conditions

It was shown in Section 2.4 that the reconstruction procedure can be extended to include the case of a duct under closed–closed end conditions. An extended series of numerical tests, whose results are not reported here for the sake of brevity, shows that the main features of the reconstruction procedure are analogous to those presented above for open–open end conditions. As an example, Fig. 13 reports the blockages identification for $N=20$, $N_e=1600$ and assuming $b=0.24$, $c=0.005$, $d=0.05$, $e=0.004$ (Fig. 13(a)) and $b=0.12$, $c=0.05$, $d=0.05$, $e=0.004$ (Fig. 13(b)).

4.8. Stability of the reconstruction to errors on the data

In this section we investigate the stability of the reconstruction algorithm when the measured frequency data are affected by errors. We assume that radian eigenfrequencies include random error defined by

$$\omega_m^{\mathrm{err}} = \omega_m + \eta\omega_1, \tag{4.6}$$

or, alternatively,

$$\omega_m^{\mathrm{err}} = \omega_m(1+\eta), \tag{4.7}$$

$m \geq 1$. Here, the number η is defined as $\eta = \eta_{\max}(2r-1)$, where r is a random number generated from a standard uniform distribution on the interval $[-1, 1]$ and $\eta_{\max}$ is the maximum error level. In Eq. (4.6), the error $\eta\omega_1$ does not depend on the mode order m and it is proportional to the fundamental frequency ω_1.

Figs. 14 and 15 report some illustrative examples of identification varying the error level $\eta_{\max}$ and the blockage depth. Results are referred to the geometric parameters $b=0.24$, $c=0.005$, and $d=0.05$; moreover, $N=20$ and $N_e=1600$. The

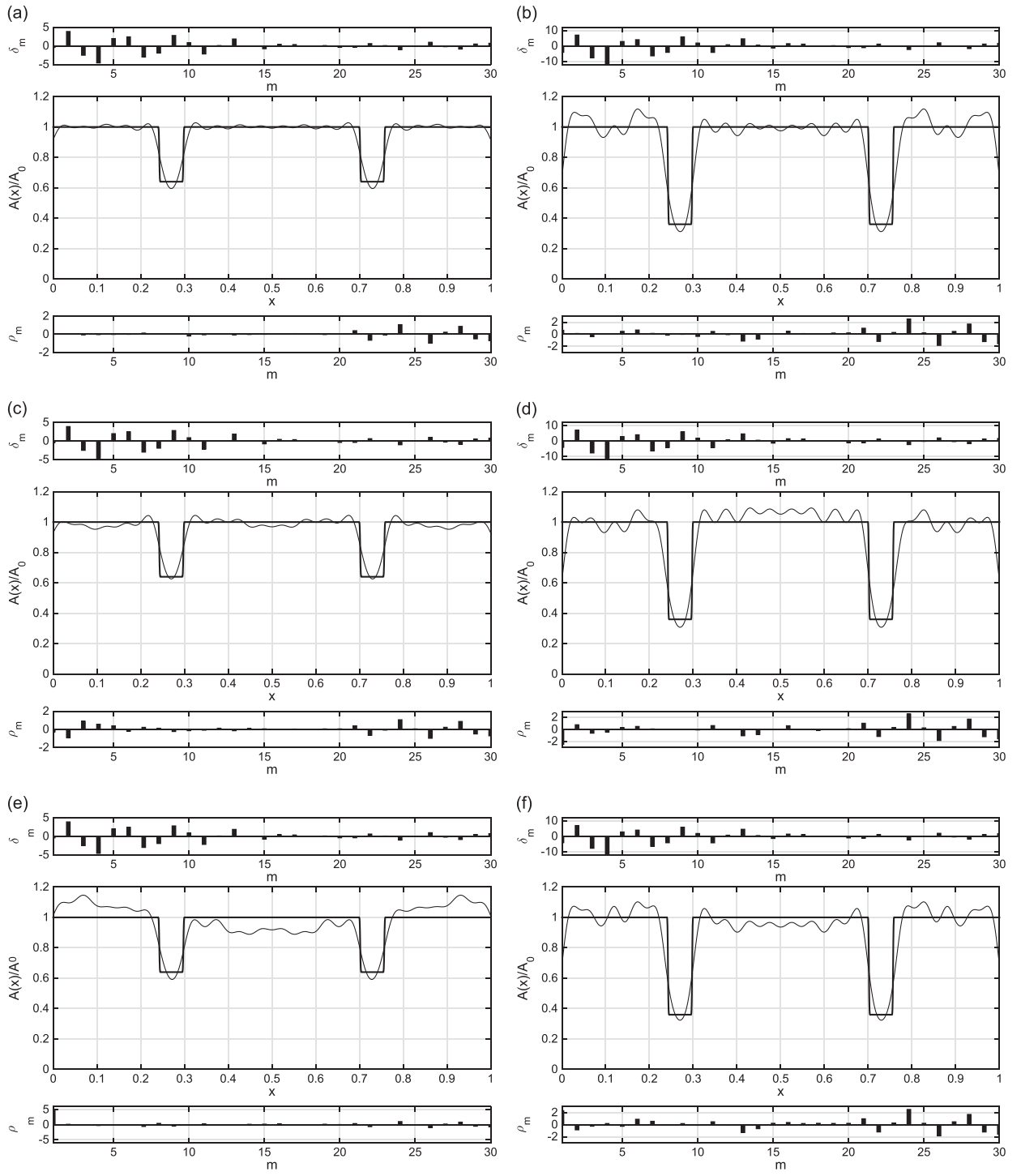

Fig. 14. Reconstruction results with errors on the data: $b=0.24$, $c=0.005$, $d=0.05$, $N=20$, $N_e=1600$, error level $\eta_{\max}$ (Eq. (4.6)). (a) $e=0.002$, $\eta_{\max}=0.01$; (b) $e=0.004$, $\eta_{\max}=0.01$; (c) $e=0.002$, $\eta_{\max}=0.03$; (d) $e=0.004$, $\eta_{\max}=0.03$; (e) $e=0.002$, $\eta_{\max}=0.05$; and (f) $e=0.004$, $\eta_{\max}=0.05$. Thick curve: exact profile; thin curve: reconstructed profile.

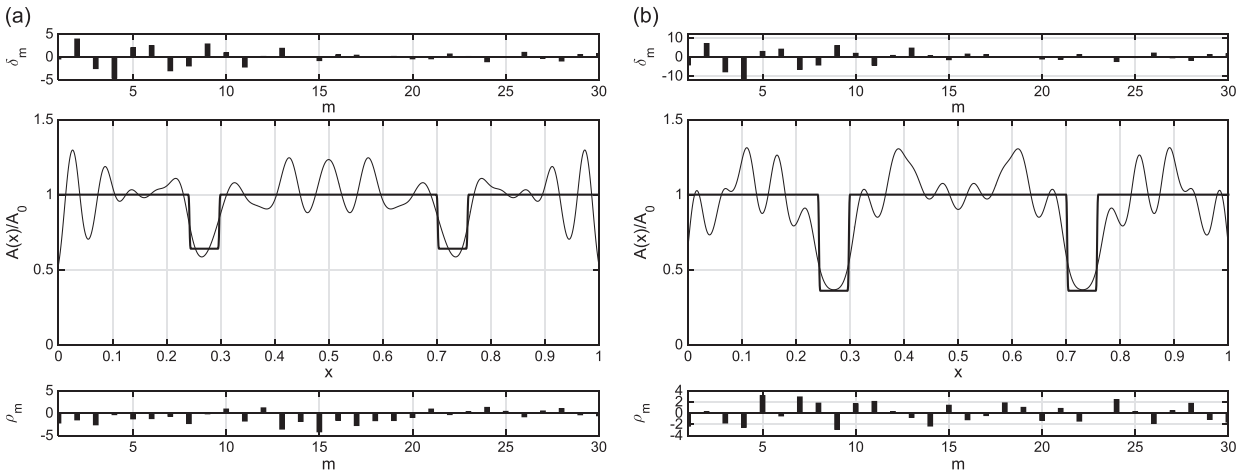

Fig. 15. Reconstruction results with errors on the data: $b=0.24$, $c=0.005$, $d=0.05$, $N=20$, $N_e=1600$, error level $\eta_{\max}=0.03$ (Eq. (4.7)). (a) $e=0.002$, $\eta_{\max}=0.03$ and (b) $e=0.004$, $\eta_{\max}=0.03$. Thick curve: exact profile; thin curve: reconstructed profile.

reconstruction turns out to be sufficiently stable and robust to errors of the type (4.6) up to $\eta_{\max}=0.05$. Conversely, the accuracy of the reconstruction is worse compared with the error-free case for errors of the type (4.7). Reconstruction is almost compromised when the duct profile to be identified is a small perturbation of the initial profile. In these cases, in fact, the eigenfrequency shifts induced by blockages are small and comparable with the errors on the data, resulting in significant difficulty on blockage identification.

4.9. No symmetric blockage

In this last section we shall investigate on possible application of the reconstruction procedure for the detection of general, *i.e.*, not necessarily symmetric profile $A=A(x)$ in an open–open duct. It is well-known that two complete spectra (and an additional scalar information on the unknown coefficient) are necessary to determine uniquely the function $A=A(x)$ in this case. Fig. 16 shows the results obtained for $N_e=1600$, $N=20$ (free-of-error data) and single blockage defined by $b=0.24$, $d=0.05$ and $e=0.004$. It is confirmed that, as expected, the reconstructed profile $A=A(x)$ is symmetric with respect to the mid-point $x=\frac{1}{2}$. However, it is interesting to notice that the identified profile shows an abrupt reduction of the cross-sectional area in a region of the interval $\left[0,\frac{1}{2}\right]$ which coincide with the actual support of the blockage. These simulations, and other not reported here for the sake of brevity, also show that the accuracy of the localization of the blockage improves in the case of small and diffuse blockages. The depth estimate, on the contrary, is rather poor and the reconstructed profile seems to suggest that the (maximum) depth is underestimated of about 50 percent.

5. Conclusions

A theoretical procedure for identifying blockages in a one-dimensional symmetric duct from a finite set of eigenfrequencies, under either open–open or closed–closed end conditions, has been presented. The identification procedure is constructive. We have shown that, starting from the unperturbed duct, it is possible to explicitly construct a duct profile having exactly the given values of the first N eigenfrequencies of the duct with blockages. The analysis is based on the determination of quasi-isospectral duct operators which have exactly the same full spectrum as a given duct, under a specified set of end conditions, with the exception of a single eigenfrequency which is free to move in a prescribed interval. The reconstruction procedure requires that the eigenfrequencies of the unperturbed duct must satisfy certain interlacing conditions with the target frequency values.

The method has been implemented numerically. An extended series of simulations leads to the following conclusions:

(i) The accuracy of the identification increases with the number of eigenfrequencies used, and better results are obtained when the lower eigenfrequencies are assigned in ascending order and the blockages are smooth and diffuse.
(ii) The reconstruction is rather stable with respect to the shape, the size and the position of the blockages; moreover, the method can be used also for identifying multiple blockages (in a half of the duct).
(iii) The additional scalar information on the unknown cross-sectional area profile (the average of the inverse of the cross-sectional area profile, in the present case) is shown to be necessary to improve the accuracy of the reconstruction.

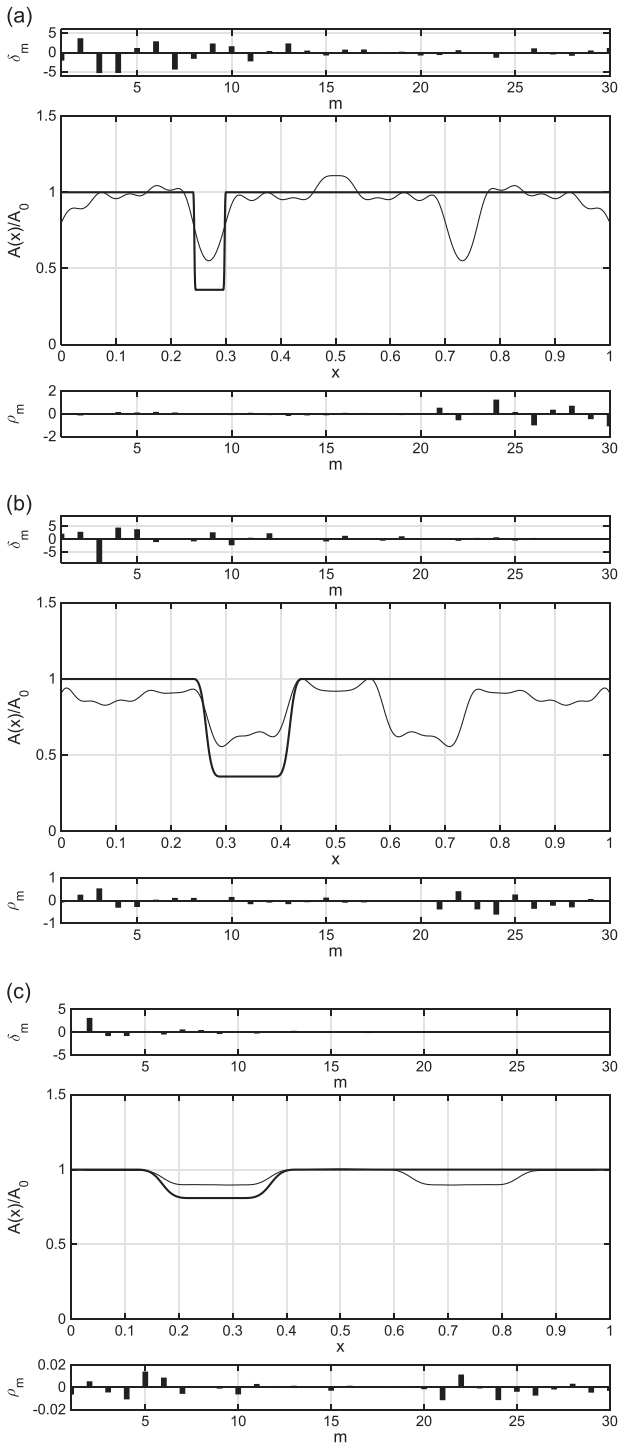

Fig. 16. Reconstruction of general blockages with $N=20$ and $N_e=1600$. (a) $b=0.24$, $c=0.005$, $d=0.05$, $e=0.004$; (b) $b=0.24$, $c=0.05$, $d=0.1$, $e=0.004$; and (c) $b=0.12$, $c=0.1$, $d=0.1$, $e=0.001$. Thick curve: exact profile; thin curve: reconstructed profile.

(iv) The method is capable to handling situations in which no-symmetric blockage is present, and for these cases a sufficiently accurate estimation of the blockage support is observed.
(v) The reconstruction procedure is sufficiently stable to errors on the eigenfrequency data.

Acknowledgements

The authors would like to thank the Referees for their constructive comments.

References

[1] M. Antonopoulos-Domis, Frequency dependence of acoustic resonances on blockage position in a fast reactor subassembly wrapper, *Journal of Sound and Vibration* 72 (4) (1980) 443–450.
[2] M.R. Schroeder, Determination of the geometry of the human vocal tract by acoustic measurements, *The Journal of the Acoustical Society of America* 41 (4) (1967) 1002–1010.
[3] P. Mermelstein, Determination of the vocal-tract shape from measured formant frequencies, *The Journal of the Acoustical Society of America* 41 (5) (1967) 1283–1294.
[4] B.H. Story, I.R. Titze, Voice simulation with a body-cover model of the vocal folds, *The Journal of the Acoustical Society of America* 97 (2) (1995) 1249–1260.
[5] B.H. Story, I.R. Titze, E.A. Hoffman, Vocal tract area functions from magnetic resonance imaging, *The Journal of the Acoustical Society of America* 100 (1) (1996) 537–554.
[6] J.M. Buick, J. Kemp, D.B. Sharp, M. van Walstijn, D.M. Campbell, R.A. Smith, Distinguishing between similar tubular objects using pulse reflectometry: a study of trumpet and cornet leadpipes, *Measurement Science and Technology* 13 (2002) 750–757.
[7] D.B. Sharp, D.M. Campbell, Leak detection in pipes using acoustic pulse reflectometry, *Acustica* 83 (1997) 560–566.
[8] A.G. Webster. Acoustical impedance and the theory of horns and of the phonograph. *Proceedings of the National Academy of Sciences of the United States of America* 5 (1919) 275–282.
[9] S.W. Rienstra, Webster's horn equation revisited, *SIAM Journal of Applied Mathematics* 65 (6) (2005) 1981–2004.
[10] G. Borg, Eine Umkehrung der Sturm-Liouvilleschen Eigenwertaufgabe. Bestimmung der Differentialgleichung durch die Eigenwerte (An inverse Sturm–Liouville eigenvalue problem. Determination of a differential equation by the eigenvalues), *Acta Mathematica* 78 (1946) 1–96.
[11] N. Levinson, The inverse Sturm–Liouville problem, *Matematisk Tidsskrift B* 32 (1949) 25–30.
[12] H. Hochstadt, On inverse problems associated with Sturm–Liouville operators, *Journal of Differential Equations* 17 (1975) 220–235.
[13] Q. Wu, F. Fricke, Determination of blocking locations and cross-sectional area in a duct by eigenfrequency shifts, *The Journal of the Acoustical Society of America* 87 (1) (1990) 67–75.
[14] M.H.F. de Salis, D.J. Oldham, Determination of the blockage area function of a finite duct from a single pressure response measurement, *Journal of Sound and Vibration* 221 (1) (1999) 180–186.
[15] M.H.F. de Salis, D.J. Oldham, The development of a rapid single spectrum method for determining the blockage characteristics of a finite length duct, *Journal of Sound and Vibration* 243 (4) (2001) 625–640.
[16] O.H. Hald, The inverse Sturm–Liouville problem with symmetric potentials, *Acta Mathematica* 141 (1978) 263–291.
[17] A. Morassi, Constructing rods with given natural frequencies, *Mechanical Systems and Signal Processing* 40 (2013) 288–300.
[18] J. Pöschel, E. Trubowitz, *Inverse Spectral Theory*, Academic Press, London, 1987.
[19] G. Darboux, Sur la répresentation sphérique des surfaces (On the spherical representation of the surfaces), *Comptes Rendus de l'Académie des Sciences Paris* 94 (1882) 1343–1345.
[20] P. Deuflhard, Recent progress in extrapolation methods for ordinary differential equations, *SIAM Review* 27 (4) (1985) 505–535.
[21] P. Henrici, *Discrete Variable Methods in Ordinary Differential Equations*, John Wiley, New York, 1962.
[22] W.B. Gragg, On extrapolation algorithms for ordinary initial value problems, *SIAM Journal on Numerical Analysis* 2 (1965) 384–404.
[23] L. Piegl, W. Tiller, *The NURBS Book*, 2nd edition, Springer-Verlag, Berlin Heidelberg, 1997.
[24] M. Aristodemo, A high continuity finite element model for two-dimensional elastic structures, *Computers and Structures* 21 (1985) 987–993.
[25] A. Bilotta, G. Formica, E. Turco, Performance of a high-continuity finite element in three-dimensional elasticity, *International Journal for Numerical Methods in Biomedical Engineering (Communications in Numerical Methods in Engineering)* 26 (2010) 1155–1175.
[26] M. Aristodemo, E. Turco, Boundary element discretization of plane elasticity and plate bending problems, *International Journal for Numerical Methods in Engineering* 37 (1994) 965–987.
[27] E. Turco, M. Aristodemo, A three-dimensional B-spline boundary element, *Computer Methods in Applied Mechanics and Engineering* 155 (1998) 119–128.
[28] A. Cazzani, M. Malagù, E. Turco, Isogeometric analysis of plane curved beams. *Mathematics and Mechanics of Solids* (April) (2014) 1–16, http://dx.doi.org/10.1177/1081286514531265.